SAND2016-9065R

SANDIA REPORT

SAND2016-xxxx
Unclassified Unlimited Release
Printed September 2016

Fukushima Daiichi Radionuclide Inventories

Jeff Cardoni and Zac Jankovsky

Prepared by
Sandia National Laboratories
Albuquerque, New Mexico 87185-0748

Sandia National Laboratories is a multi-mission laboratory managed and operated by Sandia Corporation, a wholly owned subsidiary of Lockheed Martin Corporation, for the U.S. Department of Energy's National Nuclear Security Administration under contract DE-AC04-94AL85000.

Issued by Sandia National Laboratories, operated for the United States Department of Energy by Sandia Corporation.

Available to DOE and DOE contractors from
U.S. Department of Energy
Office of Scientific and Technical Information
P.O. Box 62
Oak Ridge, TN 37831

Telephone: (865) 576-8401
Facsimile: (865) 576-5728
E-Mail: reports@adonis.osti.gov
Online ordering: http://www.osti.gov/bridge

Available to the public from
U.S. Department of Commerce
National Technical Information Service
5285 Port Royal Rd.
Springfield, VA 22161

Telephone: (800) 553-6847
Facsimile: (703) 605-6900
E-Mail: orders@ntis.fedworld.gov
Online order: http://www.ntis.gov/help/ordermethods.asp?loc=7-4-0#online

SAND2016-xxxx
Unclassified, Unlimited Release
Printed September 2016

Fukushima Daiichi Radionuclide Inventories

Jeff Cardoni and Zac Jankovsky

Sandia National Laboratories
P.O. Box 5800
Albuquerque, New Mexico 87185-0748

Abstract

Radionuclide inventories are generated to permit detailed analyses of the Fukushima Daiichi meltdowns. This is necessary information for severe accident calculations, dose calculations, and source term and consequence analyses. Inventories are calculated using SCALE6 and compared to values predicted by international researchers supporting the OECD/NEA's Benchmark Study on the Accident at Fukushima Daiichi Nuclear Power Station (BSAF). Both sets of inventory information are acceptable for best-estimate analyses of the Fukushima reactors. Consistent nuclear information for severe accident codes, including radionuclide class masses and core decay powers, are also derived from the SCALE6 analyses. Key nuclide activity ratios are calculated as functions of burnup and nuclear data in order to explore the utility for nuclear forensics and support future decommissioning efforts.

ACKNOWLEDGEMENTS

This work is funded by the US Nuclear Regulatory Commission under the purview of Don Algama and Richard Lee. Nate Andrews (SNL) is acknowledged for managing the BSAF-related research at SNL. Both he and Matt Denman (SNL) provided helpful comments and peer review of this work.

TABLE OF CONTENTS

Table of Contents ..... **v**
List of Figures ..... **vi**
Nomenclature ..... **viii**
1 Introduction **1**
1.1 Background **1**
1.2 Document Overview **3**
1.3 Section 1 References **3**
2 Nuclide Inventories **5**
2.1 Nuclear Data Libraries **5**
2.1.1 Fukushima Fuel Assemblies 5
2.1.2 Basic Reactor Operating Characteristics 6
2.1.3 Conditions for Data Library Generation 7
2.2 Nuclide Inventories for Severe Accident Analyses **10**
2.2.1 Pertinent Inputs and Assumptions 10
2.2.2 Calculated Nuclide Inventories 15
2.2.3 BSAF Comparison of Important Nuclides 20
2.3 Key Radionuclide Activity Ratios **26**
2.3.1 Dependence on Burnup and Nuclear Data 27
2.3.2 Influence of Power Level and Previous Decay Periods 31
2.3.3 Distributions of ^{134}Cs to ^{137}Cs Activity Ratio 34
2.3.4 Code Comparison of ^{134}Cs to ^{137}Cs Ratio 41
2.4 Section 2 References **42**
3 Summary and Conclusions **43**
3.1 High Level Conclusions **43**
3.2 Future Work **44**
Appendix A: Severe Accident Quantities **47**
A.1 Lumped RN Class Inventories **47**
A.2 Decay Heat **48**
A.3 Decay Power Distributions **52**
A.4 Appendix A References **53**

LIST OF FIGURES

Figure 2.1. Example Dancoff factors relative to infinite lattice value for 8x8 lattice. 8
Figure 2.2. Example TRITON/NEWT geometry models [2.6] similar to Fukushima fuel. 9
Figure 2.3. Generalized 2D BWR power distribution. 11
Figure 2.4. Generalized 2D BWR burnup distribution. 12
Figure 2.5. Unit 1 axial power and burnup distributions. 13
Figure 2.6. Unit 2 axial power and burnup distributions. 13
Figure 2.7. Unit 3 axial power and burnup distributions. 14
Figure 2.8. Axial void fraction distribution for Fukushima unit 3. 15
Figure 2.9. Actinide irradiation and decay chains [2.8] 25
Figure 2.10. TRITON and standalone ORIGEN-S predictions of ^{134}Cs:^{137}Cs ratio for unit 1. 27
Figure 2.11. TRITON and standalone ORIGEN-S predictions of ^{134}Cs:^{137}Cs ratio for unit 2. 28
Figure 2.12. TRITON and standalone ORIGEN-S predictions of ^{134}Cs:^{137}Cs ratio for unit 3. 28
Figure 2.13. ^{134}Cs:^{137}Cs ratio for various library and void fraction (0 – 50 GWd/t). 29
Figure 2.14. ^{134}Cs:^{137}Cs ratio for various library and void fraction. 30
Figure 2.15. ^{133}Cs total absorption cross section. 31
Figure 2.16. Ratio dependencies on power level and decay periods. 32
Figure 2.17. Cesium activity ratio as function of decay time (0-200 days) 33
Figure 2.18. Cesium activity ratio for long decay time (0-11 years). 33
Figure 2.19. Unit 1 assembly-averaged burnup spectrum. 34
Figure 2.20. Unit 2 assembly-averaged burnup spectrum. 35
Figure 2.21. Unit 3 assembly-averaged burnup spectrum. 35
Figure 2.22. Assembly-averaged cesium activity ratio for unit 1. 36
Figure 2.23. Assembly-averaged cesium activity ratio for unit 2. 36
Figure 2.24. Assembly-averaged cesium activity ratio for unit 3. 36
Figure 2.25. 2D spatial distribution of ^{134}Cs:^{137}Cs activity ratio. 38
Figure 2.26. 2D spatial distribution of ^{134}Cs:^{137}Cs activity ratio with listed valued. 39
Figure 2.27. ORIGEN-S and MCNP6 predictions of cesium activity ratio. 41
Figure A.1. Unit 1 decay power. 49
Figure A.2. Unit 1 decay power on severe accident time scale. 50
Figure A.3. Unit 2 decay power. 50
Figure A.4. Unit 2 decay power on severe accident time scale. 51
Figure A.5. Unit 3 decay power. 51
Figure A.6. Unit 3 decay power on severe accident time scale. 52
Figure A.7. Decay power distributions for units 1-3. 53
Figure A.8. Decay power density distributions for units 1-3. 53

LIST OF TABLES

Table 2-1. Fukushima plant data for use in SCALE6 models. 6
Table 2-2. Data library specifications from TRITON calculations. 7
Table 2-3. NEWT/TRITON model parameters. 8
Table 2-4. Noble gas primary radionuclide inventories (in Bq). 16
Table 2-5. Alkali metal primary radionuclide inventories (in Bq). 16
Table 2-6. Alkaline earth primary radionuclide inventories (in Bq). 17
Table 2-7. Halogen primary radionuclide inventories (in Bq). 17
Table 2-8. Chalcogen primary radionuclide inventories (in Bq). 17
Table 2-9. Platinoid primary radionuclide inventories (in Bq). 17
Table 2-10. Early transition metal primary radionuclide inventories (in Bq). 18
Table 2-11. Tetravalent primary radionuclide inventories (in Bq). 18
Table 2-12. Trivalent primary radionuclide inventories (in Bq). 18
Table 2-13. Key nuclide inventory comparison for unit 1. 22
Table 2-14. Key nuclide inventory comparison for unit 2. 23
Table 2-15. Key nuclide inventory comparison for unit 3. 24
Table 2-16. Predicted activity ratios for ^{134}Cs to ^{137}Cs. 26

NOMENCLATURE

ARP	Automatic Rapid Processing module in SCALE6.1.3
BWR	Boiler water reactor
CMFD	Coarse mesh finite difference
JAEA	Japan Atomic Energy Agency
LEU	Low enriched uranium
MELCOR	Sandia National Laboratories severe accident code
MOX	Mixed oxide
NEA	Nuclear Energy Agency
NEWT	Multigroup discrete ordinates transport solver in SCALE6.1.3
NRC	U.S. Nuclear Regulatory Commission
OECD	Organization for Economic Co-operation and Development
ORIGEN-S	Oak Ridge Isotope Generation code (depletion code in SCALE6.1.3)
RCS	Reactor coolant system
RN	MELCOR radionuclide package
RPV	Reactor pressure vessel
SBO	Station blackout
SNL	Sandia National Laboratories
TRITON	Coupled transport and depletion module in SCALE6.1.3

1 INTRODUCTION

Radionuclide inventories are generated to permit detailed analyses of the Fukushima Daiichi meltdowns, including severe accident calculations using MELCOR [1.1], dose calculations using MCNP6 [1.2], and consequences analysis using MACCS [1.3]. Such information is also important for Lagrangian particle dispersion predictions that are included in MACCS consequences analysis. Inventories are calculated using SCALE6[1] [1.4] in conjunction with plant data made available under the Benchmark Study on the Accident at Fukushima Daiichi Nuclear Power Station (BSAF) project [1.5]. The BSAF project is an international research effort, which includes Sandia National Laboratories (SNL), organized by the Nuclear Energy Agency (NEA) and the Organization for Economic Co-operation and Development (OECD).

The Fukushima plant data [1.5]-[1.7], some of which is proprietary, is in the form of three-dimensional distributions of power and burnup over the active core (for units 1-3) for the last cycle before the accident. Other pertinent plant data includes fuel assembly geometry, the number of fuel assembly types in each core, material compositions (e.g. MOX, enrichments, etc.), and each unit's operating history[2]. Most of this plant data is implemented as input for the SCALE6 calculations.

Radionuclide inventories are normally calculated by the plant's operating company (or a contractor) since burnup analyses are performed for each core reload. However, this information was not available to SNL from Fukushima Daiichi. Inventory information was not available initially for the BSAF project, nor were the associated decay heat curves that are also essential inputs. Hence, it is necessary to generate the information using modern tools such as SCALE6 to support severe accident research at SNL. Additional information has recently become available for the BSAF project, which permits comparison to the calculated values in this report.

A brief summary of past Fukushima research at SNL is presented in Section 1.1. This includes preliminary burnup calculations that entailed certain assumptions and approximations due to a lack of available plant information. The work described in this report seeks to improve on these past analyses using improved cross section libraries and newly available plant data. Section 1.2 provides an overview of the report content.

1.1 Background

Past SNL research related to Fukushima has focused mostly on severe accident analyses using MELCOR, and these efforts have been documented and shared with the US and international technical communities [1.8]-[1.10]. The first Fukushima models developed by SNL adopted

[1] SCALE6.1.3 is used in this report, hereafter referred to as SCALE6. The latest release, SCALE6.2, includes new tools to facilitate burnup analyses for severe accident-related research. These new tools may be considered in future work.

[2] All references herein to the “units” relate to Fukushima Daiichi unit 1, unit 2, and unit 3, which were the only reactors to undergo severe core damage following the earthquake-tsunami-induced SBO. No other reactor or spent fuel pool experienced significant fuel damage [1.8].

radionuclide and decay heat inputs from existing MELCOR models. In particular, information from the Peach Bottom SOARCA model [1.11] was used as a temporary substitute. Later, sets of representative inventory and decay heat information were created using surrogate cross section libraries to support Phase I of BSAF, which was primarily concerned with severe accident phenomenology [1.12][1.13]. This information was sufficient for the purposes of Phase I. Going forward with BSAF Phase II, which is concerned with source term forensics, involves some more detailed evaluations of radionuclide quantities using more accurate nuclear data.

Phase I of BSAF was concentrated on the characterization of plant thermal-hydraulics and severe accident phenomena at Fukushima Daiichi. This included the thermal-hydraulic transient behavior, core degradation and fuel relocation, reactor pressure vessel (RPV) lower head failure, and containment response. Such calculations require reasonable and consistent radionuclide information in the form of lumped radionuclide class masses (i.e., MELCOR RN classes), total core decay heat, and RN class decay power curves. Basic estimates of whole-core inventories of key nuclides, such as ^{131}I and ^{137}Cs, are also needed information. Therefore, depletion analyses were conducted using ORIGEN-S with surrogate cross section data in the form of pre-generated libraries that are available in SCALE6. These data libraries were reasonable proxies for the calculation of integral radionuclide quantities necessary for Phase I of BSAF. However, these libraries were generated using older ENDF/B-V nuclear data[3] and with lattice models that are not identical to the Fukushima fuel assemblies. Hence, Phase II of BSAF calls for updated depletion analyses using data libraries derived from Fukushima-specific lattice models and modern ENDF/B-VII nuclear data.

Phase II of BSAF aims to evaluate radionuclide source terms to the containment and to the environment, radionuclide transport behavior, and dose rates inside and near the plant. The radionuclide-focused goals of Phase II make use of thermal-hydraulic and severe accident insights from Phase I. The details and assumptions involved in the severe accident progression have first-order impacts on radionuclide transport and consequent dose rates.

Accurate inventories for key radionuclides are required for Phase II, since model predictions are to be benchmarked against radio-assay measurements of individual radionuclides. The inventories are also to be used in photon transport calculations for the purposes of predicting dose fields and gamma spectroscopy, for which measured data also exists for comparison and benchmarking. Photon transport analyses may play an important role in reactor decommissioning since it can provide insights on source location (i.e., where is the cesium and corium) and the radiological consequences of shielding removal. Of course, such analyses are also heavily informed by chemical and physical RN transport calculations from MELCOR.

Forensic research for Phase II may examine the activity ratios of key nuclides (e.g. ^{134}Cs to ^{137}Cs) to better understand each unit's accident progression and release characteristics. The predicted core inventories of neutron absorption products, namely ^{134}Cs for this work, are sensitive to the one-group reaction cross sections used in the depletion analyses. Thus, data libraries for each Fukushima fuel assembly type are first generated using the TRITON sequence

[3] The latest release of SCALE6 (6.2) includes improved pre-generated libraries that make use of ENDF/B-VII nuclear data. This new feature may be implemented into future BSAF work.

in SCALE6. These ENDF/B-VII-based libraries are then implemented into standalone ORIGEN-S calculations that are executed for each assembly in the cores of units 1-3 (that is, the fuel in the last operating cycle). This permits rapid and accurate evaluation of the units' distinct burnup histories in order to derive whole-core nuclide inventories.

1.2 Document Overview

This report provides a summary of burnup calculations for generating severe accident inventories and decay heat information for subsequent Fukushima research. Predicted nuclide inventories are discussed in Section 2. This section reviews TRITON calculations that generate the ENDF/B-VII-based libraries for each of the Fukushima fuel assembly types, which are implemented into the ORIGEN-S depletion analyses. The calculated nuclide quantities are compared to values provided by BSAF. Section 2 also describes detailed investigations of certain nuclide inventories that may be particularly important for source term forensics and reactor decommissioning, including the effects of burnup and cross section dependence. Conclusions and potential future work are discussed in Section 3.

The models and calculations in this report are mostly important for updating the nuclide inventories for severe accident source term analysis and related work. However, these same calculations can also produce consistent, updated information for severe accident codes like MELCOR. Appendix A presents a summary of updated RN quantities derived from the ORIGEN-S calculations, including RN class inventories and core decay powers.

1.3 Section 1 References

[1.1] L.L. Humphries, et al., "MELCOR Computer Code Manuals, Vol. 2: Reference Manuals, Version 2.1," SAND2015-6692 R, Sandia National Laboratories, Albuquerque, NM (2015).

[1.2] J.T. Goorley, et al., "MCNP6 User's Manual Version 1.0," LA-CP-13-00634, Los Alamos National Laboratory (2013).

[1.3] D.I. Chanin and M.L. Young, "Code Manual for MACCS2: Volume 1, User's Guide," NUREG/CR-6613, U.S. Nuclear Regulatory Commission, Washington, DC (1997).

[1.4] Oak Ridge National Laboratory, "Scale: A Comprehensive Modeling and Simulation Suite for Nuclear Safety Analysis and Design," ORNL/TM-2005/39, Version 6.1, June 2011. Available from Radiation Safety Information Computational Center at Oak Ridge National Laboratory as CCC-785.

[1.5] OECD/NEA, http://www.oecd-nea.org/jointproj/bsaf.html.

[1.6] TEPCO Plant Data, http://www.tepco.co.jp/nu/fukushima-np/plant-data/f1_3_Keihou3.pdf, accessed August 16 (2016).

[1.7] BSAF, Information Portal for the Fukushima Daiichi Accident Analysis and Decommissioning Activities, https://fdada.info/en/.

[1.8] R.O. Gauntt, et al., "Fukushima Daiichi Accident Study (Status as of April 2012)," SAND2012-6173, Sandia National Laboratories, Albuquerque, NM (2012).

[1.9] R.O. Gauntt, et al., "MELCOR Simulations of the Severe Accident at the Fukushima Daiichi Unit 1," *Nuclear Technology*, Vol. 186, No. 2, pp. 161-178 (2014).

[1.10] J.N. Cardoni, et al., "MELCOR Simulations of the Severe Accident at the Fukushima Daiichi Unit 3," *Nuclear Technology*, Vol. 186, No. 2, pp. 179-197 (2014).

[1.11] Sandia National Laboratories, "State-of-the-Art Reactor Consequence Analyses Project Volume 1: Peach Bottom Integrated Analysis," NUREG/CR-7110 Volume 1, USNRC, Washington, DC (2012).

[1.12] OECD/NEA, "BSAF Project: Phase I Summary Report," NEA/CSNI/R(2015)18 (2015).

[1.13] J.N. Cardoni, "Radionuclide Inventory and Decay Heat Quantification Methodology for Severe Accident Simulations," SAND2014-17667, Sandia National Laboratories, Albuquerque, NM (2014).

2 NUCLIDE INVENTORIES

Models and calculations to derive nuclide-level inventories for severe accident analyses are discussed in this section, and these predicted quantities are compared to information provided by BSAF. The bulk of the burnup analyses are accomplished using ORIGEN-S in standalone mode. Therefore, adequate data libraries must first be created that represent the Fukushima fuel assemblies and incorporate modern nuclear data such as ENDF/B-VII.1.

Section 2.1 discusses the creation of the cross section libraries for the standalone ORIGEN-S calculations. The pertinent nuclide inventories, derived from standalone burnup analyses, are presented in Section 2.2. Section 2.3 examines the burnup behavior of certain radionuclides that may be of particular importance for decommissioning and accident forensic understanding, namely ^{134}Cs and ^{137}Cs.

2.1 Nuclear Data Libraries

Problem dependent cross section data is used in the burnup calculations. These data libraries are generated using the TRITON sequence in SCALE6. The accurate prediction of radionuclide information depends on the proper implementation of one-group cross sections that are weighted by the problem-dependent neutron flux. The unique geometric and material aspects of fuel assemblies, in addition to different operating conditions (e.g. power history, void fraction, and temperature), influence the spatial and spectral distribution of the neutron flux over the fuel lattice; this affects the one-group cross sections that are used in depletion analyses. The creation of new data libraries for the Fukushima fuel assemblies includes the implementation of the latest ENDF/B-VII.1 nuclear data.

2.1.1 Fukushima Fuel Assemblies

According to publically available information [2.1]-[2.3], there were five major fuel assembly types in the cores of Fukushima units 1-3 during the last operating cycles. These assembly designs differ by lattice arrangement (e.g. 8x8 vs 9x9), fuel rod diameter and spacing (pitch), water rod size and position, burnable poison zoning, material properties (e.g. enrichment, MOX, etc.), and overall length; such differences affect the one-group cross sections needed by ORIGEN-S.

Fukushima Daiichi unit 1 contained two major fuel types: the 9x9B assembly (i.e. STEP3B) and older 8x8 (i.e. STEP2) assemblies. Fukushima unit 2 is comprised entirely of the 9x9B/STEP3B assemblies, except with greater axial length compared to unit 1. Fukushima Daiichi unit 3 contained two major fuel types: the 9x9A assembly, also referred to as STEP3A, and 8x8 MOX fuel assemblies, which are geometrically similar to the STEP2 (non-MOX) assemblies used in unit 1 except some rods contain mixed oxide (MOX) fuel. Detailed schematics of the fuel assemblies are provided in SAND2014-3966 [2.4].

2.1.2 Basic Reactor Operating Characteristics

The necessary Fukushima plant data used as SCALE6 input is mostly available publically via the Tokyo Electric Power Company (TEPCO) and BSAF data websites [2.1][2.3][2.5]. Some of the information used is proprietary or only available to BSAF members, such as the more detailed design information for the fuel assemblies, and this information is omitted here. The information that is publically available is listed below and summarized in Table 2-1:

- Overall BOC and EOC burnups, power levels, and cycle operating times;
- General fuel assembly design (e.g. BWR 9x9) and average enrichments;
- Core and assembly fuel loading, i.e. metric tons of uranium;
- Two-dimensional (axial/radial) power and burnup distributions, from collapsed 3D data;
- Two-dimensional layouts of the core fuel assemblies;
- Axial void fraction distribution for full-power operation.

Table 2-1. Fukushima plant data for use in SCALE6 models.

	Fukushima Unit 1	Fukushima Unit 2	Fukushima Unit 3
Reactor type	BWR/3	BWR/4	BWR/4
Rating (MWt)	1380	2381	2381
Fuel mass (tHM)	68	94	94
# fuel assemblies	400	548	548
# control blades	97	137	137
Final operating time before accident (days) (1)	191	113	169
Core-avg. BOC burnup (GWd/t) (2)	21.95	20.17	17.22
Core-avg. EOC burnup (GWd/t) (2)	25.78	22.95	21.41
Peak fuel assembly burnup (GWd/t) (2)	41.3	42.4	41.7
Specific power (MW/t)	20.3	25.6	25.6
Fuel assemblies – type (quantity)	8x8 (68), 9x9B (332)	9x9B (548)	9x9A (516), 8x8MOX (32)
Average enrichment (w/o)	8x8: 3.4 9x9B: 3.6	3.8	9x9A: 3.8 8x8MOX: 1.2 ^{235}U 8x8MOX: 3.9 Pu(3)

(1) Fukushima units 1-3 appear to have operated on cycles durations ranging from 300 days to 520 days, according to publically available outage and fuel offload histories.
(2) This burnup data is from the plant process computer (e.g., [2.1]), which is publically available.
(3) This is the total plutonium weight percent in the MOX fuel rods. The plutonium vector is currently unknown, but is likely proprietary.

Table 2-1 describes some basic information on reactor parameters for Fukushima units 1-3. This data, in addition to some more detailed plant information, is implemented as input for TRITON models of each unique fuel assembly. This includes geometric and material inputs for NEWT 2D deterministic transport models. Some of this information is also utilized in the standalone ORIGEN-S calculations discussed in Section 2.2.

Unit 1 is a significantly smaller reactor in terms of number of fuel assemblies, fuel load, and power level, and it is an older BWR/3 design; however, it had the highest burnup per ton of initial fuel at shutdown. Units 2 and 3 are similar units with the same power level. The initial fuel loading and the operating time of the current cycle affects the end of cycle (EOC) core. Unit 3 operated longer than unit 2 before the accident (169 days vs. 113 days), but the beginning of cycle burnup (BOC) for unit 2 was higher. Hence, the EOC burnup of unit 2 exceeds that of unit 3. The EOC burnup is an essential figure that determines nuclide inventories (particularly longer-lived radionuclides), lumped radionuclide class inventory masses for MELCOR, and long-term decay heat. The overall power level and the most recent operating history, such as the number of days into the current cycle, are more important in determining the decay power soon after shutdown and the inventory of short-lived radionuclides.

2.1.3 Conditions for Data Library Generation

Problem-dependent cross sections and modern ENDF/B-VII.1 nuclear data are incorporated into the burnup analyses. ORIGEN-S/ARP data libraries are generated using the TRITON sequence in SCALE6.1.3. TRITON inputs decks are created for each of the (five) unique fuel assemblies in units 1-3 and for the following conditions detailed in Table 2-2 below.

Table 2-2. Data library specifications from TRITON calculations.

TRITON model input	**Input value(s)**
Assembly-averaged burnup	0 – 72 GWd/t
Specific power level	unit 1 fuel: 20.3 MW/t, unit 2/3 fuel: 25.6 MW/t
^{235}U enrichment	2.4 – 5.0 w/o (unit 3 MOX: 1.2 – 2.5 w/o)
^{239}Pu content (unit 3 MOX only)	3.2 – 59 w/o
Coolant void fraction	0 – 90%
Coolant density	0.1 – 0.74 g/cm^3 (corresponding to the void fraction)
Fuel temperature	900 K
Cladding (Zircaloy-2) temperature	600 K
Water temperature	553 K
Burnable poison (Gd_2O_3) in lattice	With and without Gd_2O_3 in the lattice
B_4C control blade	Rodded and un-rodded plane

The TRITON models burn all fuel material by constant power depletion–the fuel is burned uniformly (i.e., separate fuel materials are not defined for each rod location). The ENDF/B-VII 238 group library is used ("v7-238") along with CENTRM for cross section processing, which is the one-dimensional discrete ordinates option in SCALE for calculating point-wise energy spectra and preparing the problem-dependent, multigroup data library [2.6]; thus each assembly model uses a unique, self-shielded 238 group library for the NEWT deterministic transport calculations in the TRITON sequence.

Cases with void fraction over 75% implement Dancoff factors derived using the MCDancoff module in SCALE6 [2.6]. BWR lattices with low moderation can exhibit rod-shadowing effects for resonance energy neutrons, particularly for rods along the lattice edges, which need to be accounted for in the resonance self-shielding calculations performed before the lattice transport

solution [2.7]. Unique Dancoff factors are generated for each assembly type, and are approximated to be constant with depletion. Figure 2.1 provides an example of some calculated Dancoff factors for an 8x8 BWR lattice with 50% void; the blue bar reflects the position of the control blade. The values in Figure 2.1 are relative to the infinite lattice value (i.e., D_{inf} / D_{local}) that was calculated to be about 0.2595. This figure demonstrates how rods near the edge of the lattice, including near the central water rod, exhibit Dancoff factors that are significantly different than the infinite lattice value. Lattice calculations with higher void fraction leads to greater deviation from the infinite lattice Dancoff value [2.7].

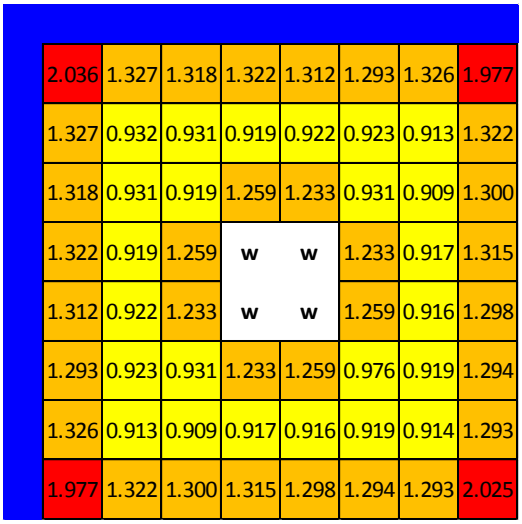

Figure 2.1. Example Dancoff factors relative to infinite lattice value for 8x8 lattice.

Additional numerical parameters for TRITON and NEWT are listed in Table 2-3. The transport calculations use coarse mesh finite difference acceleration, which accelerates convergence of the iterative solvers in NEWT. Two fine-mesh cells per coarse cell are specified for CMFD in both the x- and y-directions. Convergence criteria for eigenvalue (epseigen) and inner/outer spatial (epsinner/epsouter) convergence are reasonable for the purposes of this work, while also not incurring excessive CPU costs. The order of the level symmetric quadrature set is set to the default value. The addnux=3 option is specified to incorporate a sufficient number of nuclides in trace quantities. For depletion codes it is often necessary to add trace amounts (e.g. $1x10^{-20}$ atom/barn-cm) of fission products, decay products, and activation products in order to readily assess the impact of cross sections and reaction rates evolving as a function of burnup [2.6].

Table 2-3. NEWT/TRITON model parameters.

Input parameter	Description	Value
cmfd	Coarse mesh finite difference acceleration	Yes
xcmfd	Fine-mesh cells per coarse-mesh cell (x-direction)	2
ycmfd	Fine-mesh cells per coarse-mesh cell (y-direction)	2
epseigen	Convergence for k_{eff}	$1x10^{-5}$
epsinner	Spatial convergence criterion for inner iterations	$1x10^{-4}$
epsouter	Spatial convergence criterion for outer iterations	$1x10^{-4}$
sn	Order of Sn level symmetric quadrature set	6
addnux	Additional nuclides for depletion	3

To further expedite the TRITON calculations, the 'weight' option is implemented that allows for a broader 49 energy-group structure to be used for the majority of each depletion calculation. That is, the first transport solution uses the 238 group library, which is then collapsed to a 49 group library using the problem-averaged (whole-assembly) flux. Hence, subsequent transport calculations for the remaining time steps use the broader cross section library to significantly decrease CPU time. This introduces some biases in the calculation, but the effect should be negligible for the purposes of assembly-averaged cross sections and whole-core radionuclide inventories for severe accidents [2.6][2.7].

Currently, the radionuclide inventory calculations in Section 2.2 only make use of the libraries from the un-rodded TRITON models. Plant information on control rod position is rather limited, and the inventory calculations are conducted for each individual fuel assembly irrespective of any axial nodes. Future analyses can investigate higher-fidelity, 3D methods that explicitly treat control rod position and void fraction distribution. The libraries with burnable poison are also not implemented due to limited information of core fuel/poison zoning. The Gd_2O_3 burnable poison might change the neutron spectrum enough to impact the reaction rates of key neutron capture products such as ^{134}Cs. This is another potential avenue for future investigations.

Figure 2.2 shows example TRITON/NEWT geometry representations 9x9 and 8x8 BWR lattices that are grossly comparable to the Fukushima fuel assemblies; these assemblies are generic BWR templates available with the SCALE6 installation and are described in the code manual [2.6]. The actual lattice models for the Fukushima fuel are not shown here since doing so may reveal proprietary information. The illustrations in Figure 2.2 are analogous, but the actual models have a finer mesh, incorporate more details for the control blade, and have slightly different water rod placement. For planar calculations with no poison blade, which are most important for depletion calculations, the control blade materials are replaced with water in the models. The 9x9B (STEP3B) in units 1 and 2 have slight geometric differences, as do the 8x8 (STEP2 and MOX) assemblies in units 1 and 3. The TRITON models account for the key differences between the assembly types such as the lattice (8x8 vs. 9x9) and the position/size of the water rod(s), which act to increase moderation and thermal flux in the center of the lattice.

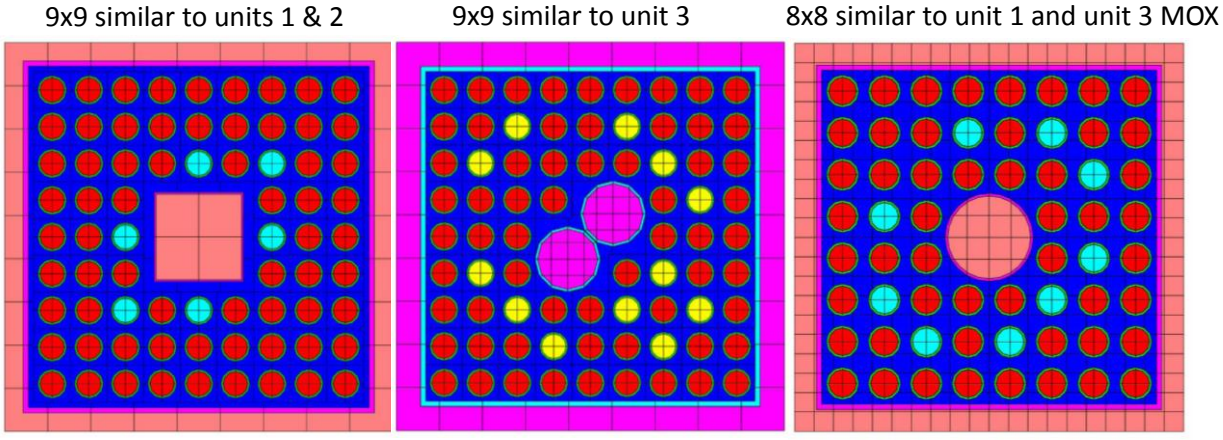

Figure 2.2. Example TRITON/NEWT geometry models [2.6] similar to Fukushima fuel.

2.2 Nuclide Inventories for Severe Accident Analyses

Burnup analyses using ORIGEN-S in SCALE6.1.3 to generate nuclide inventories for Fukushima units 1-3 are presented in this section. The calculations are conducted for each fuel assembly present in the final cycles of each reactor–that is, an ORIGEN-S input file is created and executed for each assembly. This allows for reasonably detailed accounting of the 2D radial power and burnup profiles over the cores. Axial variations are currently neglected in these calculations. It is assumed that axially-integrated quantities of (local) assembly power and void fraction are sufficient for generating integral severe accident quantities, such as whole-core inventories. The Automatic Rapid Processing (ARP) module is also used in these calculations to interpolate enrichment, burnup, and void fraction over the ORIGEN-S data libraries, which are generated at discrete increments of these variables.

The predicted whole-core nuclide inventories are presented here and compared to values provided by BSAF. The BSAF inventories were generated by the Japan Atomic Energy Agency (JAEA) using similar methods, namely ORIGEN2 with appropriate cross section libraries. However, many details and assumptions incorporated by the JAEA analyses are currently unknown, as much of the pertinent documentation is only available in Japanese [2.3].

2.2.1 Pertinent Inputs and Assumptions

Many of the inputs used in the TRITON models (Table 2-1) are also necessary inputs for the ORIGEN-S standalone calculations. This includes the basic reactor parameters such as power level, fuel load, number of assemblies and assembly types, average enrichments, and operating history. Moreover, the ORIGEN-S calculations use unit-specific plant data for the last operating cycle in the form of 3D power and burnup distributions. The 3D plant data is integrated into 2D information for each fuel assembly. Data is also available for the axial distribution of void fraction in the cores, and this data is used to inform a single representative void fraction that determines which cross sections to use in the calculations.

Figure 2.3 depicts a 2D, axially-integrated power distribution over a typical BWR core. Each fuel assembly has its own distinct power fraction in this figure. It is not direct plant data, but rather post-processed and generalized information to illustrate the basic features of a modern BWR power distribution (thus the omission of a numerical scale for the color contour). The red assemblies signify above-average relative power fraction, while the blue assemblies denote below average power; the yellowish regions are near the assembly-average power fraction for the core. The z-elevation in Figure 2.3 also reflects relative assembly power. The flat dark-blue regions are empty (i.e. outside the nearly-cylindrical active core region). There exists some significant local heterogeneity in assembly-to-assembly power fraction, yet the global 2D power distribution is basically center-peaked. Assuming a typical 5-ring MELCOR core model, such data reduces to a center-peaked distribution where the inner three rings have comparable power densities, and the outer two rings have significantly lower power [2.4].

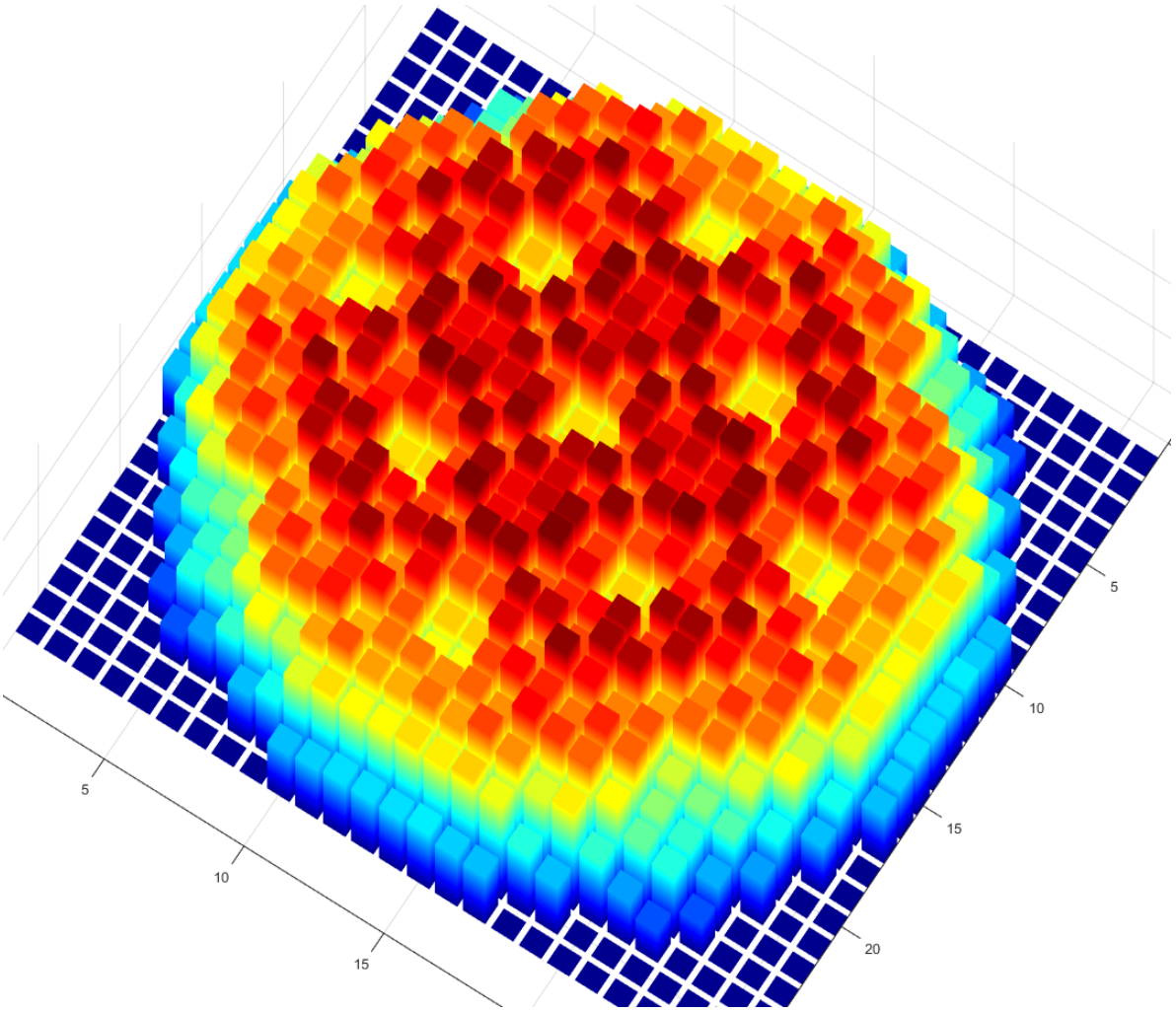

Figure 2.3. Generalized 2D BWR power distribution.

A comparable generic figure of burnup distribution is given by Figure 2.4. In contrast to the power distribution, the 2D radial burnup distribution is highly heterogeneous due to fuel shuffling. The central core region is largely a checkerboard pattern of burnup, which would simply be homogenized when integrated into 1D MELCOR core rings. The outer ring of fuel assemblies are exclusively higher burnup (mostly accrued during previous cycles), yet these assemblies have relatively low operating power as seen in Figure 2.3. Thus, the outer core ring in a MELCOR model might have lower decay power, but it would contain relatively high concentrations of long-lived and stable nuclides for key RN classes such as ^{127}I, ^{129}I, ^{133}Cs, and ^{137}Cs.

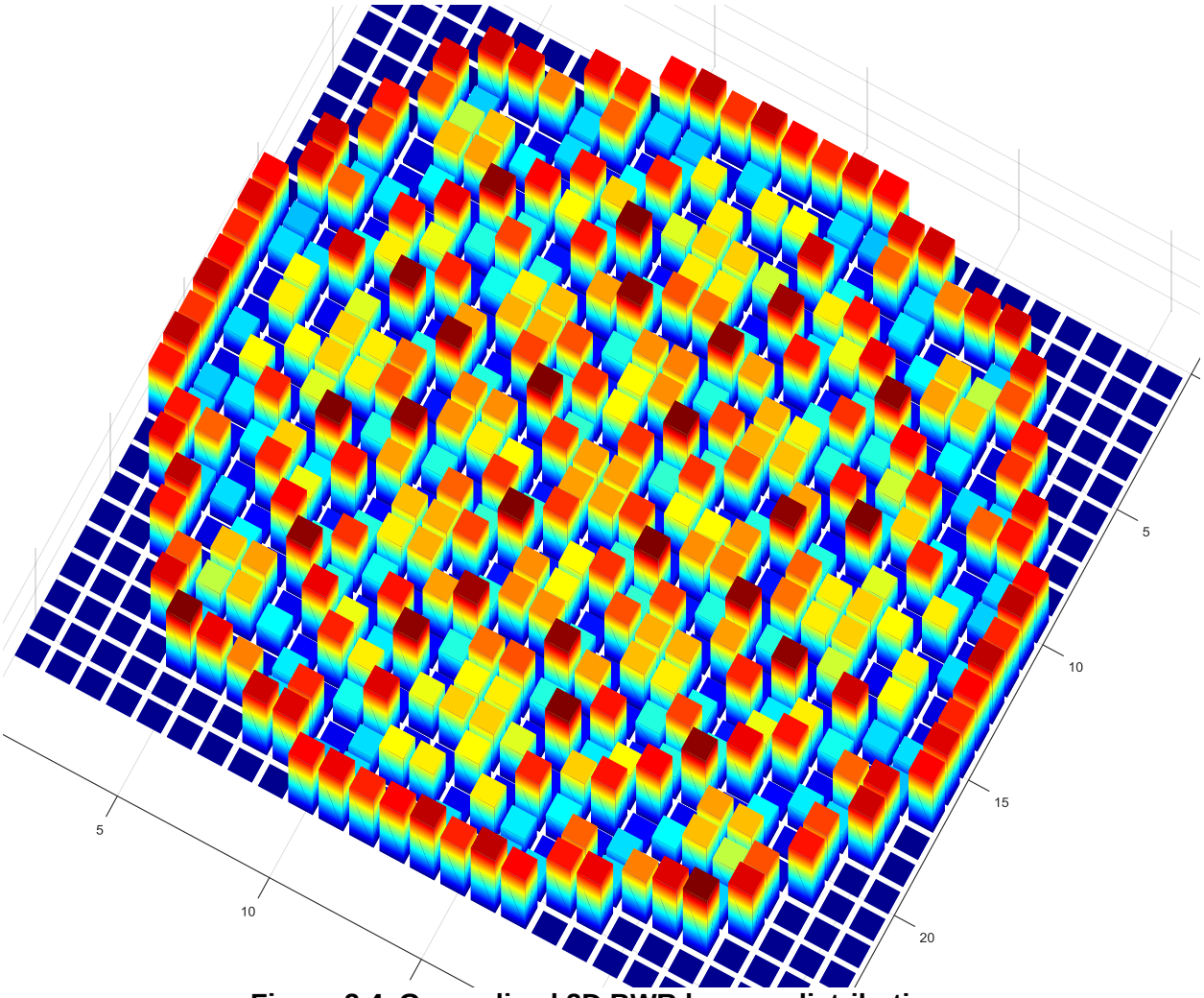

Figure 2.4. Generalized 2D BWR burnup distribution.

Figure 2.5, Figure 2.6, and Figure 2.7 show the axial distributions (normalized to the averages) of power and burnup for unit 1, unit 2, and unit 3, respectively. Also depicted on these figures are nodal factors that can be implemented into severe accident models for the purposes of specifying decay power distribution and allocating nodal RN class masses. The axial distributions of operating power and burnup distributions are intrinsically similar; this is the natural result of the axial symmetry of the core and the lack of axial fuel shuffling. Hence, nodal RN masses in MELCOR may be allocated to either the axial power distribution or the axial burnup distribution, and the differences should be second order at most. The decay power soon after shutdown follows the operating power distribution, since high power regions of the core contain higher concentrations of short-lived nuclides. Conversely, lumped RN class masses are dominated by long-lived and stable nuclides that intrinsically build with burnup.

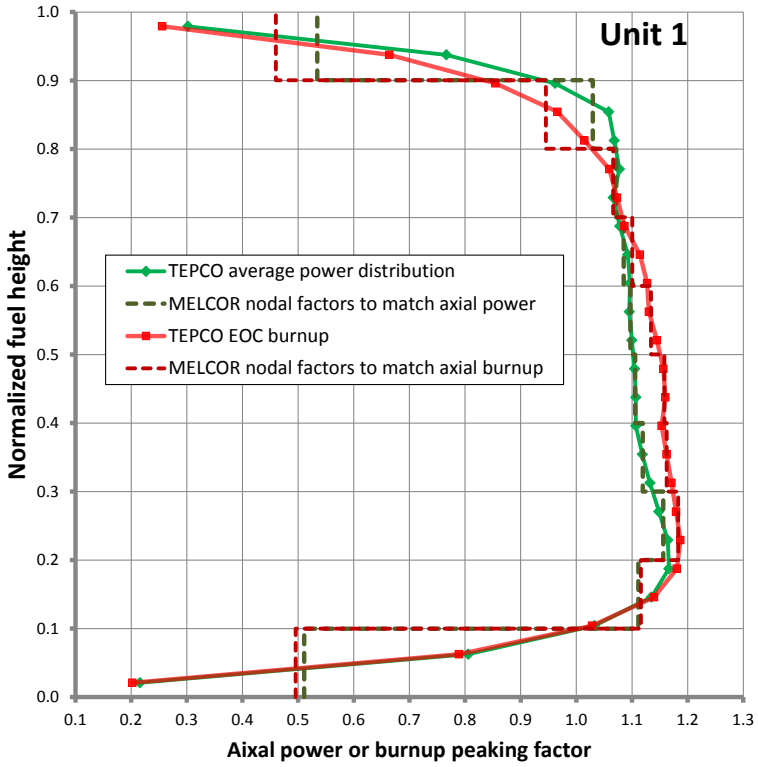

Figure 2.5. Unit 1 axial power and burnup distributions.

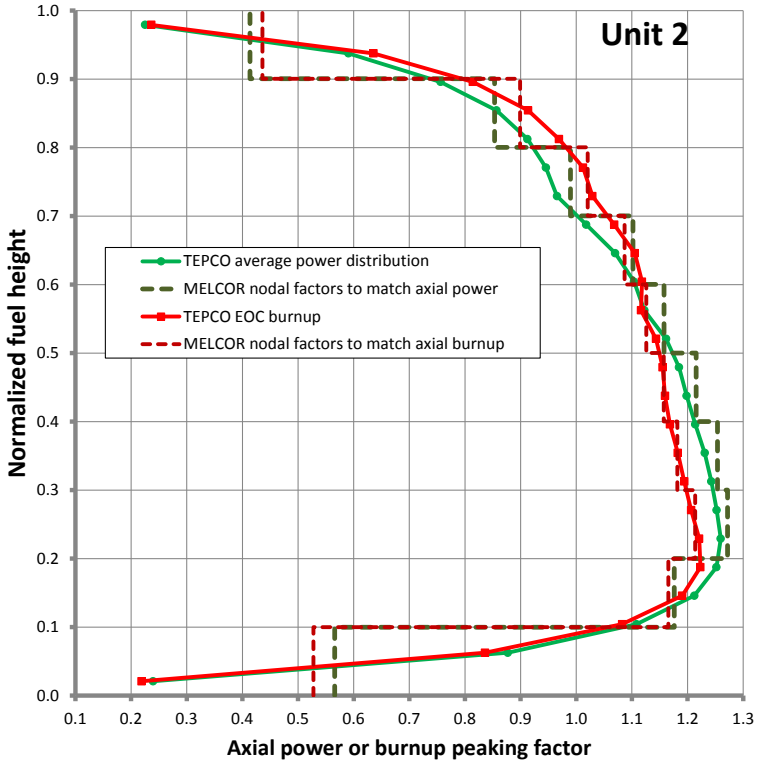

Figure 2.6. Unit 2 axial power and burnup distributions.

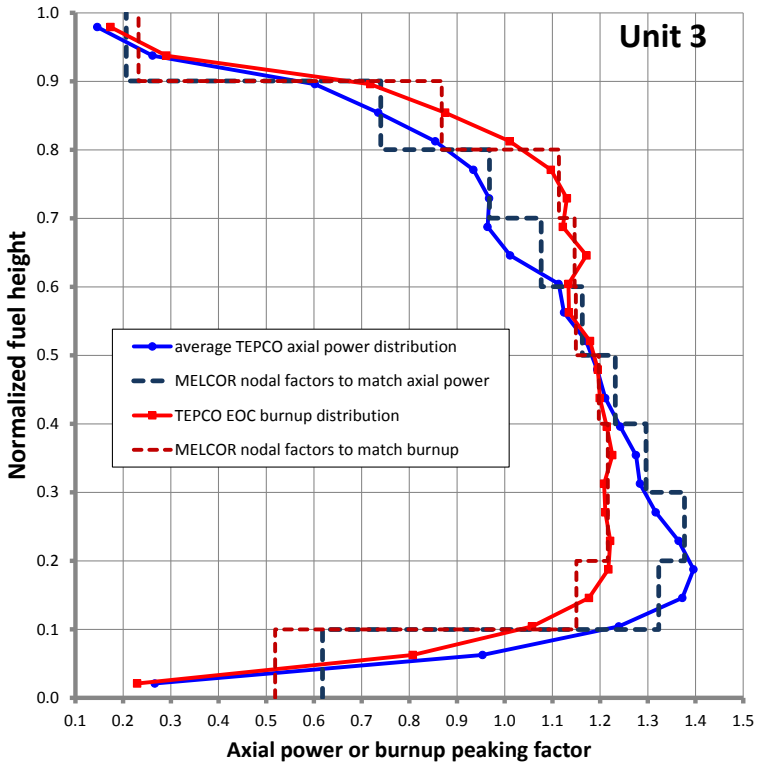

Figure 2.7. Unit 3 axial power and burnup distributions.

A major simplification in the ORIGEN-S analyses is the use of axially-integrated values for assembly power and void fraction. Spatial heterogeneity in power and burnup distributions for LWRs is largely radial due to fuel shuffling and the axial symmetry of the core. For instance, by comparing the 2D radial distributions (Figure 2.3 and Figure 2.4) to the 1D axial distributions for each unit (Figure 2.5, Figure 2.6, and Figure 2.7), it is apparent that the axial power/burnup distributions are essentially a distorted cosine shape, while the radial distributions exhibit relatively large assembly-to-assembly variability.

However, BWRs are designed for two-phase flow through the active region of the core, and hence there is an axial distribution of void fraction (and thus coolant/moderator density) that has important influences on the spectral and spatial characteristics of neutron reaction rates. Coolant enters the bottom of the core in a subcooled state and is heated to the bulk saturation temperature after traversing about 10% of the active fuel length. After saturation, additional heat is transferred to the coolant by increased void formation as the coolant rises and exits the core. Steam voids affect the bulk density of the coolant/moderator, and therefore significantly influence neutron flux. These effects are considered in detail for rigorous reactor analyses that aim to predict reactivity, neutron transport/balance, and power distributions. But for the standalone ORIGEN-S calculations in this work, which simply ‘infer’ radionuclide inventories associated with known reactor operation and the given plant data, 2D analyses that use problem-dependent cross section libraries from TRITON are reasonable. The spatial and spectral characteristics of each assembly are considered by the spatially-integrated, one-group cross sections given to ORIGEN-S.

Void fraction in the active core region generally ranges from 0.0 at the inlet to about 0.7 at the core exit, as shown by Figure 2.8. It depicts the operating void distribution for Fukushima unit 3 during its final cycle before the severe accident, and is publically accessible from the TEPCO website [2.1]. The effective void fraction implemented into the ORIGEN-S analyses can be a simple axially-integrated value, a power- or burnup-weighted value, or even a parameter that can be adjusted to facilitate agreement with other predictions (such as the BSAF values).

A void fraction of 0.3 is assumed to be representative of the core void distribution in the ORIGEN-S calculations for each unit. This void fraction is used to calculate an average moderator density for the analyses using the following formula:

$$\rho_{avg} = \alpha\rho_v + \rho_l(1-\alpha)$$

Where,
ρ_{avg} = Bulk average density of the two-phase mixture
α = Average void fraction
ρ_v = Vapor (i.e., steam/void) density at saturation temperature
ρ_l = Liquid density at saturation temperature.

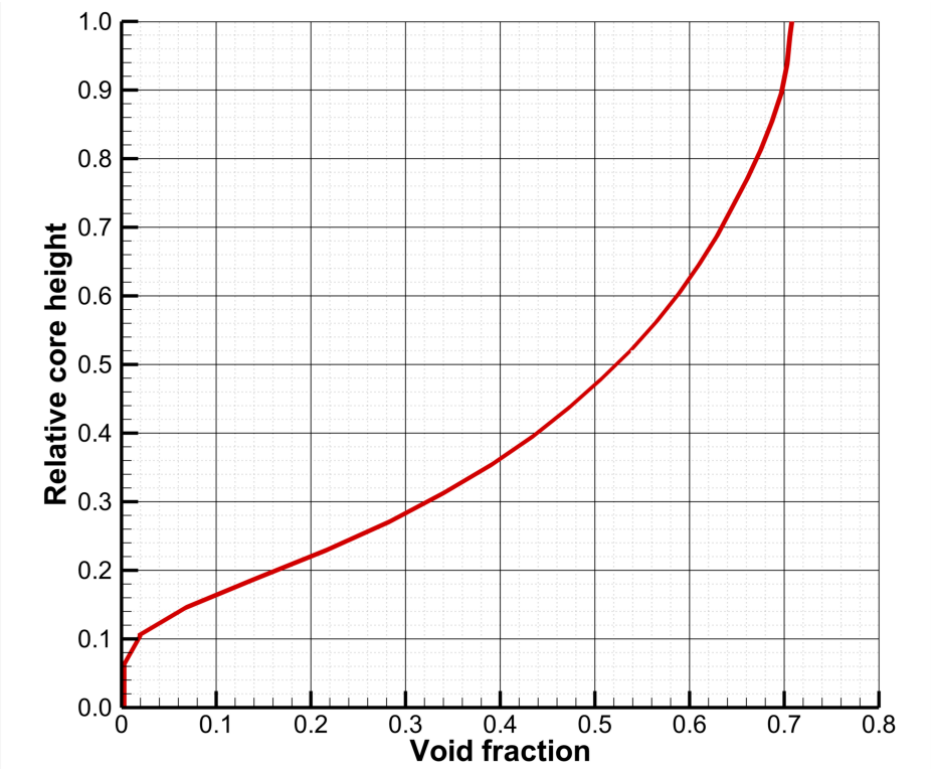

Figure 2.8. Axial void fraction distribution for Fukushima unit 3.

2.2.2 Calculated Nuclide Inventories

The predicted radionuclide inventories for Fukushima units 1-3 are presented here. Activities of radionuclides most important for severe accident consequences are tabulated for each unit –

these are compared to the BSAF values in the next section (2.2.3). Only essential radionuclides are listed in this section, but the whole-core inventories calculated by ORIGEN-S also include corresponding sets of nuclide mass inventories for stable isotopes (the activity of a stable isotope is zero). Nuclide masses are important for the summation of RN class masses for chemical and physical radionuclide transport calculations in severe accident codes like MELCOR. Stable nuclides are inherently significant contributors to gross RN class masses, since stable nuclides build continuously with burnup and do not decay (the only loss mechanism being neutron transmutation).

The following tables list activities (in Becquerels) separated by MELCOR RN class for principal severe accident radionuclides. The inventory tables by class are:

- Noble gases, with representative element Xe, are listed in Table 2-4;
- Alkali metals, with representative element Cs, are listed in Table 2-5;
- Alkaline earths, with representative element Ba, are listed in Table 2-6;
- Halogens, with representative element I, are listed in Table 2-7;
- Chalcogens, with representative element Te, are listed in Table 2-8;
- Platinoids, with representative element Ru, are listed in Table 2-9;
- Early transition metals, with representative element Mo, are listed in Table 2-10;
- Tetravalents, with representative element Ce, are listed in Table 2-11;
- Trivalents, with representative element La, are listed in Table 2-12.

Table 2-4. Noble gas primary radionuclide inventories (in Bq).

Isotope	Unit 1	Unit 2	Unit 3
Kr-85	1.94E+16	2.55E+16	2.40E+16
Kr-85m	4.12E+17	7.27E+17	7.05E+17
Kr-87	8.23E+17	1.46E+18	1.41E+18
Kr-88	1.09E+18	1.94E+18	1.87E+18
Xe-133	2.88E+18	4.98E+18	4.97E+18
Xe-135	8.39E+17	1.47E+18	1.60E+18
Xe-135m	5.95E+17	1.02E+18	1.03E+18

Table 2-5. Alkali metal primary radionuclide inventories (in Bq).

Isotope	Unit 1	Unit 2	Unit 3
Cs-134	1.93E+17	2.71E+17	2.47E+17
Cs-136	4.45E+16	6.82E+16	7.05E+16
Cs-137	2.01E+17	2.52E+17	2.36E+17
Rb-86	1.78E+15	3.00E+15	2.99E+15
Rb-88	1.11E+18	1.96E+18	1.90E+18

Table 2-6. Alkaline earth primary radionuclide inventories (in Bq).

Isotope	Unit 1	Unit 2	Unit 3
Ba-137m	1.91E+17	2.39E+17	2.25E+17
Ba-139	2.59E+18	4.49E+18	4.46E+18
Ba-140	2.50E+18	4.32E+18	4.30E+18
Sr-89	1.42E+18	2.34E+18	2.43E+18
Sr-90	1.53E+17	1.95E+17	1.83E+17
Sr-91	1.88E+18	3.33E+18	3.23E+18
Sr-92	2.00E+18	3.53E+18	3.43E+18

Table 2-7. Halogen primary radionuclide inventories (in Bq).

Isotope	Unit 1	Unit 2	Unit 3
I-131	1.36E+18	2.33E+18	2.35E+18
I-132	2.03E+18	3.51E+18	3.52E+18
I-133	2.85E+18	4.91E+18	4.91E+18
I-134	3.25E+18	5.62E+18	5.60E+18
I-135	2.72E+18	4.70E+18	4.69E+18

Table 2-8. Chalcogen primary radionuclide inventories (in Bq).

Isotope	Unit 1	Unit 2	Unit 3
Te-127	1.06E+17	1.77E+17	1.85E+17
Te-127m	9.69E+15	1.53E+16	1.70E+16
Te-129	3.35E+17	5.63E+17	5.81E+17
Te-129m	5.08E+16	8.25E+16	8.88E+16
Te-131	1.18E+18	2.03E+18	2.04E+18
Te-131m	2.42E+17	4.07E+17	4.20E+17
Te-132	1.95E+18	3.36E+18	3.38E+18

Table 2-9. Platinoid primary radionuclide inventories (in Bq).

Isotope	Unit 1	Unit 2	Unit 3
Ru-103	1.89E+18	3.02E+18	3.27E+18
Ru-105	1.23E+18	2.00E+18	2.13E+18
Ru-106	5.75E+17	8.71E+17	8.64E+17
Rh-103m	1.87E+18	2.99E+18	3.24E+18
Rh-105	1.10E+18	1.89E+18	2.02E+18
Rh-106	6.37E+17	9.83E+17	9.74E+17

Table 2-10. Early transition metal primary radionuclide inventories (in Bq).

Isotope	Unit 1	Unit 2	Unit 3
Co-58	3.63E+13	6.11E+13	6.28E+13
Co-60	6.10E+15	7.75E+15	7.21E+15
Mo-99	2.61E+18	4.51E+18	4.50E+18
Tc-99m	2.30E+18	3.97E+18	3.97E+18
Nb-95	2.04E+18	3.23E+18	3.55E+18
Nb-97	2.43E+18	4.22E+18	4.19E+18
Nb-97m	2.30E+18	3.99E+18	3.96E+18

Table 2-11. Tetravalent primary radionuclide inventories (in Bq).

Isotope	Unit 1	Unit 2	Unit 3
Ce-141	2.32E+18	3.84E+18	3.98E+18
Ce-143	2.25E+18	3.92E+18	3.87E+18
Ce-144	1.51E+18	2.50E+18	2.49E+18
Np-239	2.28E+19	3.93E+19	3.96E+19
Pu-238	3.30E+15	3.98E+15	5.49E+15
Pu-239	5.36E+14	7.79E+14	1.03E+15
Pu-240	8.59E+14	1.04E+15	1.47E+15
Pu-241	1.65E+17	2.28E+17	2.93E+17
Zr-95	2.24E+18	3.64E+18	3.87E+18
Zr-97	2.41E+18	4.19E+18	4.16E+18

Table 2-12. Trivalent primary radionuclide inventories (in Bq).

Isotope	Unit 1	Unit 2	Unit 3
Am-241	3.25E+14	3.27E+14	3.52E+14
Cm-242	5.93E+16	6.83E+16	6.59E+16
Cm-244	2.77E+15	3.30E+15	2.76E+15
La-140	2.55E+18	4.40E+18	4.38E+18
La-141	2.36E+18	4.03E+18	4.07E+18
La-142	2.29E+18	3.98E+18	3.95E+18
Nd-147	9.21E+17	1.59E+18	1.59E+18
Y-90	1.57E+17	1.99E+17	1.87E+17
Y-91	1.80E+18	2.95E+18	3.09E+18
Y-92	2.02E+18	3.57E+18	3.48E+18
Y-93	2.23E+18	3.91E+18	3.83E+18
Y-91m	1.11E+18	1.99E+18	1.91E+18
Pr-143	2.25E+18	3.91E+18	3.87E+18
Pr-144	1.52E+18	2.51E+18	2.51E+18
Pr-144m	2.02E+16	3.46E+16	3.39E+16

By examining the tables above it is apparent that units 2 and 3, the larger reactors in terms of power level and fuel loading, generally have larger inventories of radionuclides. The population of longer-lived[4] radionuclides, in particular those with low absorption cross section, is directly proportional to burnup and the overall size of the reactor, or more precisely the integral energy generation (i.e. burnup in GWd/t multiplied by the fuel load in metric tons); therefore long-lived isotopic inventories are also proportional to the integral number of fissions. This effect is evident in the tables for key longer-lived fission products such as ^{85}Kr ($t_{1/2} \approx 10.8$ years), ^{137}Cs ($t_{1/2} \approx 30.2$ years), and ^{90}Sr ($t_{1/2} \approx 28.9$ years), and neutron absorption products such as ^{134}Cs ($t_{1/2} \approx 2$ years), ^{242}Cm ($t_{1/2} \approx 163$ days), and ^{244}Cm ($t_{1/2} \approx 18.1$ years). Unit 2 has slightly larger inventories of these nuclides owing to its slightly higher burnup than unit 3 (about 23 GWd/t vs. 21.4 GWd/t, respectively). The rate of burnup (specific power level), operating history including shutdown times, and cross section effects also have substantial impacts on these nuclide quantities. It is noted that although unit 1 is the smaller reactor it had the greatest per fuel burnup of 25.8 GWd/t. Hence, the long-lived nuclide inventories in unit 1 are relatively high given its power level and fuel load: Unit 1 had a power level of 1380 MW and 68 t of uranium, compared to 2381 MW and 94 t of uranium for units 2 and 3. If one were to downscale the unit 2 and 3 inventories of long-lived nuclides by the power level or fuel load compared to unit 1 (i.e. $1380/2381 \approx 0.58$ or $68/94 \approx 0.72$), the downscaled values would underestimate the true unit 1 values. In fact, some long-lived nuclides in unit 1 such as ^{244}Cm actually exceed the inventory in unit 3. This demonstrates the importance of explicitly considering burnup in generating severe accident inventories.

In contrast to the longer-lived radionuclides, short-lived isotopes and those with significant absorption cross section reach saturation concentrations and do not build monotonically with burnup. The equilibrium concentrations of such nuclides depend on the individual half-lives and cross section, in addition to the rate of production from fission, neutron absorption, and decay in-growth. The production mechanisms are largely proportional to the reactor power level, and thus unit 2 and 3 possess higher inventories of short-lived isotopes compared to unit 1. Examples include the pertinent iodine isotopes in Table 2-7, including ^{131}I with ~8 day half-life, and several other short-lived nuclides that are important for severe accident such as:

- ^{133}Xe ($t_{1/2} \approx 5.2$ days),
- ^{140}Ba ($t_{1/2} \approx 12.8$ days) and its decay daughter ^{140}La ($t_{1/2} \approx 1.7$ days),
- ^{129}Te ($t_{1/2} \approx 70$ min), ^{129m}Te ($t_{1/2} \approx 33.6$ days), ^{131}Te ($t_{1/2} \approx 25$ min), ^{131m}Te ($t_{1/2} \approx 33$ hours), and ^{132}Te ($t_{1/2} \approx 3.2$ days),
- ^{239}Np ($t_{1/2} \approx 2.4$ days), which is an important decay heat contributor,
- ^{99}Mo ($t_{1/2} \approx 2.7$ days),
- ^{97}Zr ($t_{1/2} \approx 16.7$ hours), and
- ^{147}Nd ($t_{1/2} \approx 11$ days).

The equilibrium concentrations of short-lived nuclides can vary slightly with reactor operation due to changing effective yields, actinide buildup, and cross section variations with burnup.

[4] The term 'longer-lived' is used here relative to severe accident time frames (days to many weeks), while short-lived refers to half-lives on the order of days or less, such as ^{131}I with $t_{1/2} \approx 8$ days.

Nevertheless, these nuclides are mostly a function of power level when comparing the whole-core inventories across the Fukushima units. It is for this reason that the unit 2 and 3 quantities of short-lived nuclides are nearly identical, despite unit 2 having a ~7% higher burnup.

The calculated plutonium inventories for unit 3 explicitly consider the 32 MOX assemblies in its core. The MOX assemblies generally have a minimal impact on integral quantities for severe accident information, given that the MOX only comprises 32/548 ≈ 6% of the core and each MOX assembly is a blend of LEU and MOX fuel. However, due to its MOX unit 3 does possess more plutonium content than unit 2.

2.2.3 BSAF Comparison of Important Nuclides

Predicted quantities of some critical nuclides for severe accidents are compared to BSAF values calculated by JAEA. A rigorous, in-depth analysis of differences and similarities between the two sets of information is not completed here, mainly due to limited details of the assumptions and approximations used in the JAEA calculations. It is only known that the JAEA inventories were calculated using ORIGEN2. A detailed comparison of the predicted quantities of each nuclide is a laborious effort that requires the following information:

- One-group cross sections, the raw cross section library used to generate the cross sections for ORIGEN (e.g. ENDF/B-V, ENDF/B-VII, JEFF-3.1, JENDL-4.0, etc.), and the methods, approximations, and assumptions implemented in the lattice analyses such as single fuel pin model vs. 2D assembly model.
- The specifics of the problem-independent nuclear library used in the analysis, which includes data such as decay constants, fission yields, decay mode probabilities, and particle emission energies.
- Modeling approach for the ORIGEN depletion calculations: whole-core depletion (i.e. one ORIGEN input model), calculations by fuel batches (i.e. separate ORIGEN input decks for fresh fuel, once-burned fuel, twice-burned fuel, etc.), assembly-level calculations, or 3D depletion.
- Numerous assumptions and approximations for the ORIGEN calculations including: average void fractions, accounting of burnable poisons (e.g. Gd_2O_3), modeling of previous irradiation cycles and decay periods, and the modeling fidelity of the last operating cycle.

Table 2-13, Table 2-14, and Table 2-15 compare inventories of some radionuclides that are crucial for severe accidents; these tables list the JAEA- and SNL-calculated activities for unit 1, unit 2, and unit 3, respectively. Also included in these tables are an older (circa-2011) inventory calculation performed by TEPCO that was intended to support initial Fukushima research and preliminary efforts for BSAF. Like the JAEA inventory, the TEPCO information was also generated using ORIGEN2, and the details of the analysis (e.g. nuclear data, void fraction, modeling approach) are largely unknown.

In the tables below, the “TEPCO vs. JAEA” and the “JAEA vs. SNL” columns list the percent differences of each predicted nuclide activity between the respective calculations. The JAEA and SNL inventories are very agreeable for most important nuclides such as ^{134}Cs, ^{137}Cs, ^{90}Sr, iodine

isotopes including ^{131}I, and ^{132}Te. The difference in calculated quantities for these nuclides is generally less than 2%. Such close agreement is important for using either inventory for source term analyses and the use of activity ratios in accident forensics (i.e. ^{134}Cs to ^{137}Cs ratio). Generally good agreement also exists for other significant fission products between the JAEA and SNL analyses, as most differences are less than 10%.

Some key nuclides exhibit over 15% difference when comparing the JAEA and SNL inventories, and there is no constant trend of over- or under-prediction (some SNL values exceed the JAEA values, others do not). It is currently impractical to decipher the exact causes for these noteworthy but reasonable disparities. Many of these nuclides, specifically actinides like plutonium and curium, have several modes of production and removal, and hence these quantities are more sensitive to differences in nuclear data libraries and modeling assumptions. This is quite opposite the simpler accounting necessary for fission products like ^{137}Cs, which is produced mostly from fission and has a relatively low neutron absorption cross section. Hence, assuming two analyses implement similar fission yields (the yield of an important nuclide like ^{137}Cs is well-characterized) and irradiate the fuel to the same burnup, the predicted quantities of the fission product should be comparable.

Table 2-13. Key nuclide inventory comparison for unit 1.

Nuclide	TEPCO (Bq)	JAEA (Bq)	SNL (Bq)	TEPCO vs. JAEA (%)	JAEA vs. SNL (%)
Kr 87	7.24E+17	7.73E+17	8.23E+17	6.38	6.43
Kr 88	1.02E+18	1.08E+18	1.09E+18	5.39	1.11
Xe 133	2.78E+18	2.71E+18	2.88E+18	2.82	6.43
Xe 135	1.19E+18	1.05E+18	8.39E+17	13.92	20.00
Xe 135m	5.43E+17	6.04E+17	5.95E+17	10.08	1.52
Cs 134	2.76E+17	1.90E+17	1.93E+17	45.01	1.45
Cs 137	1.97E+17	2.02E+17	2.01E+17	2.66	0.60
Rb 88	1.04E+18	1.10E+18	1.11E+18	6.08	0.69
Sr 90	1.41E+17	1.50E+17	1.53E+17	5.50	2.25
Ba 139	2.52E+18	2.54E+18	2.59E+18	0.95	2.00
Ba 140	2.42E+18	2.52E+18	2.50E+18	3.81	0.78
I 131	1.36E+18	1.35E+18	1.36E+18	1.05	0.94
I 132	1.97E+18	1.99E+18	2.03E+18	0.95	2.17
I 133	2.80E+18	2.84E+18	2.85E+18	1.31	0.39
I 134	3.08E+18	3.17E+18	3.25E+18	2.64	2.66
I 135	2.62E+18	2.69E+18	2.72E+18	2.47	1.28
Te 127	1.42E+17	1.03E+17	1.06E+17	37.34	2.73
Te 127m	1.86E+16	8.15E+15	9.69E+15	128.34	18.85
Te 129	4.25E+17	4.12E+17	3.35E+17	3.28	18.67
Te 129m	6.33E+16	4.40E+16	5.08E+16	43.91	15.55
Te 131	1.21E+18	1.12E+18	1.18E+18	8.08	5.46
Te 131m	1.95E+17	3.12E+17	2.42E+17	37.50	22.45
Te 132	1.94E+18	1.95E+18	1.95E+18	0.67	0.09
Ru 103	2.05E+18	1.88E+18	1.89E+18	8.85	0.37
Rh 105	1.30E+18	1.18E+18	1.10E+18	9.96	6.93
Mo 99	2.57E+18	2.57E+18	2.61E+18	0.23	1.72
Nb 95	2.29E+18	1.90E+18	2.04E+18	20.46	7.42
Ce 141	2.30E+18	2.26E+18	2.32E+18	1.90	2.57
Ce 143	2.14E+18	2.21E+18	2.25E+18	2.92	1.85
Np 239	2.81E+19	2.53E+19	2.28E+19	10.77	9.99
Pu 238	5.90E+15	4.63E+15	3.30E+15	27.61	28.67
Pu 239	7.45E+14	7.01E+14	5.36E+14	6.26	23.54
Pu 240	8.77E+14	8.87E+14	8.59E+14	1.10	3.15
Pu 241	2.62E+17	2.23E+17	1.65E+17	17.24	26.11
Am 241	4.04E+14	5.62E+14	3.25E+14	28.07	42.14
Cm 242	8.27E+16	8.91E+16	5.93E+16	7.25	33.47
Cm 244	5.56E+15	2.71E+15	2.77E+15	105.55	2.32

Table 2-14. Key nuclide inventory comparison for unit 2.

Nuclide	TEPCO (Bq)	JAEA (Bq)	SNL (Bq)	TEPCO vs. JAEA (%)	JAEA vs. SNL (%)
Kr 87	1.35E+18	1.36E+18	1.46E+18	0.59	7.68
Kr 88	1.90E+18	1.89E+18	1.94E+18	0.45	2.34
Xe 133	4.87E+18	4.67E+18	4.98E+18	4.42	6.62
Xe 135	1.87E+18	1.58E+18	1.47E+18	18.32	7.22
Xe 135m	9.36E+17	1.03E+18	1.02E+18	9.55	1.63
Cs 134	3.44E+17	2.76E+17	2.71E+17	24.59	1.83
Cs 137	2.43E+17	2.55E+17	2.52E+17	4.84	1.45
Rb 88	1.93E+18	1.94E+18	1.96E+18	0.38	1.37
Sr 90	1.79E+17	1.91E+17	1.95E+17	6.30	2.01
Ba 139	4.45E+18	4.40E+18	4.49E+18	1.16	2.14
Ba 140	4.24E+18	4.35E+18	4.32E+18	2.68	0.67
I 131	2.34E+18	2.34E+18	2.33E+18	0.17	0.34
I 132	3.42E+18	3.43E+18	3.51E+18	0.22	2.45
I 133	4.91E+18	4.90E+18	4.91E+18	0.15	0.17
I 134	5.42E+18	5.47E+18	5.62E+18	0.95	2.71
I 135	4.59E+18	4.64E+18	4.70E+18	1.01	1.26
Te 127	2.32E+17	1.74E+17	1.77E+17	33.48	1.85
Te 127m	2.82E+16	1.21E+16	1.53E+16	132.16	26.36
Te 129	7.14E+17	6.99E+17	5.63E+17	2.10	19.51
Te 129m	1.02E+17	7.06E+16	8.25E+16	44.56	16.95
Te 131	2.09E+18	1.93E+18	2.03E+18	8.63	5.50
Te 131m	3.32E+17	5.28E+17	4.07E+17	37.06	22.96
Te 132	3.37E+18	3.36E+18	3.36E+18	0.24	0.06
Ru 103	3.26E+18	3.00E+18	3.02E+18	8.79	0.60
Rh 105	2.05E+18	1.91E+18	1.89E+18	7.33	1.16
Mo 99	4.49E+18	4.43E+18	4.51E+18	1.33	1.78
Nb 95	3.54E+18	2.94E+18	3.23E+18	20.48	9.91
Ce 141	3.87E+18	3.72E+18	3.84E+18	4.24	3.38
Ce 143	3.83E+18	3.83E+18	3.92E+18	0.06	2.25
Np 239	4.65E+19	4.32E+19	3.93E+19	7.66	8.84
Pu 238	6.39E+15	4.57E+15	3.98E+15	39.81	12.91
Pu 239	9.21E+14	8.83E+14	7.79E+14	4.27	11.77
Pu 240	1.04E+15	1.04E+15	1.04E+15	0.50	0.69
Pu 241	3.09E+17	2.81E+17	2.28E+17	9.70	18.90
Am 241	3.72E+14	4.35E+14	3.27E+14	14.35	24.72
Cm 242	8.50E+16	8.94E+16	6.83E+16	4.97	23.64
Cm 244	5.49E+15	3.21E+15	3.30E+15	70.68	2.53

Table 2-15. Key nuclide inventory comparison for unit 3.

Nuclide	TEPCO (Bq)	JAEA (Bq)	SNL (Bq)	TEPCO vs. JAEA (%)	JAEA vs. SNL (%)
Kr 87	1.32E+18	1.33E+18	1.41E+18	0.34	6.29
Kr 88	1.87E+18	1.85E+18	1.87E+18	0.80	1.00
Xe 133	4.86E+18	4.67E+18	4.97E+18	4.20	6.55
Xe 135	1.90E+18	1.65E+18	1.60E+18	15.12	3.20
Xe 135m	9.47E+17	1.04E+18	1.03E+18	9.21	1.37
Cs 134	3.18E+17	2.52E+17	2.47E+17	26.32	1.81
Cs 137	2.32E+17	2.41E+17	2.36E+17	3.60	2.13
Rb 88	1.89E+18	1.89E+18	1.90E+18	0.01	0.11
Sr 90	1.71E+17	1.81E+17	1.83E+17	5.12	1.09
Ba 139	4.44E+18	4.38E+18	4.46E+18	1.54	1.94
Ba 140	4.27E+18	4.35E+18	4.30E+18	1.71	1.01
I 131	2.37E+18	2.33E+18	2.35E+18	1.85	1.13
I 132	3.44E+18	3.43E+18	3.52E+18	0.35	2.63
I 133	4.93E+18	4.90E+18	4.91E+18	0.64	0.29
I 134	5.43E+18	5.46E+18	5.60E+18	0.54	2.61
I 135	4.60E+18	4.63E+18	4.69E+18	0.64	1.35
Te 127	2.38E+17	1.78E+17	1.85E+17	33.68	4.29
Te 127m	2.90E+16	1.33E+16	1.70E+16	118.20	28.13
Te 129	7.29E+17	7.11E+17	5.81E+17	2.58	18.24
Te 129m	1.06E+17	7.48E+16	8.88E+16	42.38	18.80
Te 131	2.11E+18	1.93E+18	2.04E+18	9.33	5.79
Te 131m	3.38E+17	5.40E+17	4.20E+17	37.31	22.15
Te 132	3.39E+18	3.37E+18	3.38E+18	0.67	0.24
Ru 103	3.41E+18	3.25E+18	3.27E+18	4.84	0.70
Rh 105	2.13E+18	2.03E+18	2.02E+18	4.92	0.81
Mo 99	4.49E+18	4.42E+18	4.50E+18	1.59	1.75
Nb 95	3.75E+18	3.33E+18	3.55E+18	12.81	6.84
Ce 141	4.00E+18	3.89E+18	3.98E+18	2.76	2.25
Ce 143	3.82E+18	3.80E+18	3.87E+18	0.30	1.66
Np 239	4.57E+19	4.30E+19	3.96E+19	6.32	7.96
Pu 238	7.59E+15	5.53E+15	5.49E+15	37.09	0.84
Pu 239	1.15E+15	1.04E+15	1.03E+15	10.45	1.30
Pu 240	1.44E+15	1.36E+15	1.47E+15	5.72	8.04
Pu 241	3.36E+17	3.15E+17	2.93E+17	6.61	7.05
Am 241	1.48E+15	5.58E+14	3.52E+14	165.82	37.04
Cm 242	1.72E+17	1.04E+17	6.59E+16	65.96	36.53
Cm 244	4.80E+15	2.71E+15	2.76E+15	77.34	1.79

Figure 2.9 illustrates the more complicated mechanisms of actinide production and removal. For instance, the inventory of ^{239}Pu depends on its neutron cross sections for fission, radiative capture (n, γ), and absorption with emission of two neutrons (n, 2n). It is also a function of the neutron reactions with ^{238}Pu (n, γ) and ^{240}Pu (n, 2n). Lastly, ^{239}Pu undergoes alpha decay with a half-life of about 24,100 years, and it receives decay in-growth from ^{239}Np via beta decay and ^{243}Cm via alpha decay. Therefore, it is apparent that the use of different nuclear data in independent analyses can easily lead to rather sizable inventory differences for actinides. For the unit 1 and unit 2 calculations, the JAEA and SNL inventories of plutonium differ by 10-30% excluding ^{240}Pu that only has 0.7-3% difference. The plutonium inventories for unit 3 are in better agreement with differences less than 10%, which suggests that the MOX cross section libraries (generated by TRITON) used in the SNL analyses were reasonably accurate. Inventories for other key nuclides such as ^{241}Am and ^{242}Cm differ by 20-40% – the largest discrepancy being ^{241}Am in unit 1. However, the inventories for ^{244}Cm are in good agreement for each unit with less than 3% differences. ^{244}Cm and ^{242}Cm are vital for characterization of spontaneous fission neutrons in shutdown reactors, and hence accurate initial inventories will be important when comparing predicted neutron dose rates to the plant measurements during the accidents.

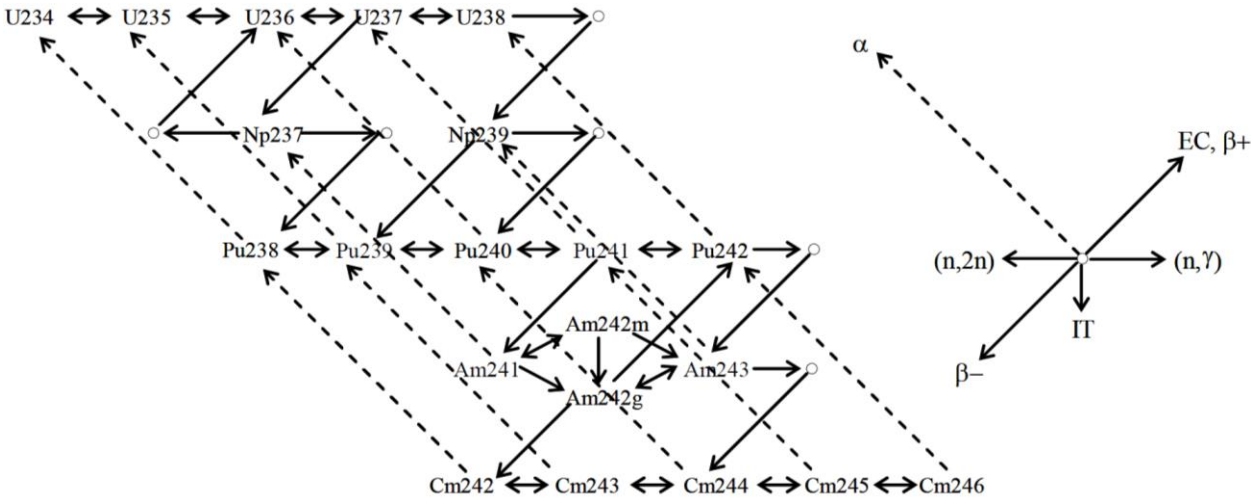

Figure 2.9. Actinide irradiation and decay chains [2.8].

Other significant disparities between the JAEA and SNL inventories exist for some of the tellurium isotopes and isomers. Predicted activities for ^{127}Te and ^{132}Te are in close agreement, but other tellurium nuclides differ by over 15%. This is probably indicative of different nuclear data being utilized in the two analyses, namely fission yields and/or decay data. Nonetheless the JAEA and SNL inventories are in reasonably gross agreement – no nuclide activity differs by more than 42% and the median percent difference for the tabulated nuclides is only 3%.

The JAEA-SNL differences are deemed reasonable given that the other Japanese analysis by TEPCO generally yields larger differences. For example, the TEPCO inventory of ^{127m}Te differs by more than 100% of the JAEA value for all three units. Furthermore, the inventory of important fission products like ^{134}Cs and ^{137}Cs have larger relative differences. The 25% and higher discrepancy between the TEPCO and JAEA inventories of ^{134}Cs might reflect different

absorption cross sections for ^{133}Cs, an important stable fission product due to its mass contribution to the alkali metal class and the fact that its neutron transmutation creates ^{134}Cs. ^{134}Cs has no decay in-growth since ^{134}Xe is stable, and thus the discrepancy must be the result of one or more of the following variables: different ^{133}Cs inventory (perhaps due to different fission yields), different neutron capture cross section for ^{133}Cs (e.g. different nuclear data library or different assumed void fraction), and different burnup modeling assumption such as the treatment of previous irradiation and decay cycles. The fact that two analyses that used the same code (ORIGEN2) could produce such unique inventories for the same reactors demonstrates the sensitivities of burnup calculations to nuclear data and modeling assumptions, and it provides some context of what constitutes acceptable agreement for severe accident information.

2.3 Key Radionuclide Activity Ratios

Forensic research for BSAF Phase II may examine the activity ratios of key nuclides (e.g. ^{134}Cs to ^{137}Cs) to better understand each unit's accident progression and release characteristics. For example, activity measurements from cesium deposition can yield estimates of localized ^{134}Cs to ^{137}Cs activity ratio. The measured ratios may then be compared to the distinct ratios of each unit, since units 1-3 have unique burnups and other operating characteristics that influence the ratio. Therefore, the nuclear characteristics of each plant, in conjunction with deposition measurements, might be able to decipher which unit was responsible for the distinctive releases and deposition patterns. It is of fundamental forensic and scientific interest to determine which unit was responsible for the various plumes exhibited by the deposition data, particularly the largest plume to the northwest of the plant. Such insights might also inform future mitigation strategies for severe nuclear accidents.

However, there are challenges and potential complications to this approach. According to burnup analyses, whole-core ratios only differ by about 3% between units 2 and 3, and by about 10-13% between units 1 and 2, as summarized in Table 2-16. The inventory of ^{134}Cs is sensitive to numerous modeling assumptions and approximations, including burnup history and the one-group reaction cross sections used in the depletion analysis. Furthermore, the measured activity data exhibits a rather large spread in measured ^{134}Cs to ^{137}Cs ratio, which either reflects the considerable heterogeneity of assembly burnup within each core and/or measurement uncertainty; BSAF and TEPCO information specified that some of the activity measurements were near the detection limit, and thus potentially unreliable. Nonetheless, the use of nuclear code predictions and nuclear measurement data for accident forensics is a novel idea that necessitates rigorous technical investigation.

Table 2-16. Predicted activity ratios for ^{134}Cs to ^{137}Cs.

Reactor	SNL value	JAEA value
Unit 1	0.964	0.941
Unit 2	1.079	1.083
Unit 3	1.048	1.044

This section explores some of the dependencies and sensitivities of ^{134}Cs to ^{137}Cs ratio as a function of burnup and nuclear data (Section 2.3.1). The influences of void fraction and base

nuclear data (i.e., ENDF/B-V vs. ENDF/B-VII) are examined. Power level and the effects of decay time are discussed in Section 2.3.2. Distributions of cesium ratio over the Fukushima reactors are presented in Section 2.3.3. A code comparison of predicted cesium ratio is given by Section 2.3.4.

2.3.1 Dependence on Burnup and Nuclear Data

The sensitivities of ^{134}Cs to ^{137}Cs activity ratio are explored in this section using ORIGEN-S in conjunction with ARP. These calculations use cross section data that is derived from TRITON analyses (Section 2.1). TRITON can also be used directly to calculate the inventory ratio, albeit at increased computational expense since it performs deterministic transport solutions between the depletion steps. The standalone ORIGEN-S and TRITON predictions are logically very similar, as shown by Figure 2.10, Figure 2.11, and Figure 2.12 for units 1, 2, and 3, respectively. These figures compare TRITON calculations of ^{134}Cs to ^{137}Cs ratio to those using ORIGEN-S in standalone mode. The ORIGEN-S predictions are within 1% of the TRITON predictions, and the bias grows slightly with higher burnups. This demonstrates that faster ORIGEN-S calculations may be used to evaluate the nuclide ratio in lieu of coupled transport-depletion simulations (which are slower), assuming that ORIGEN-S has access to appropriate cross section data.

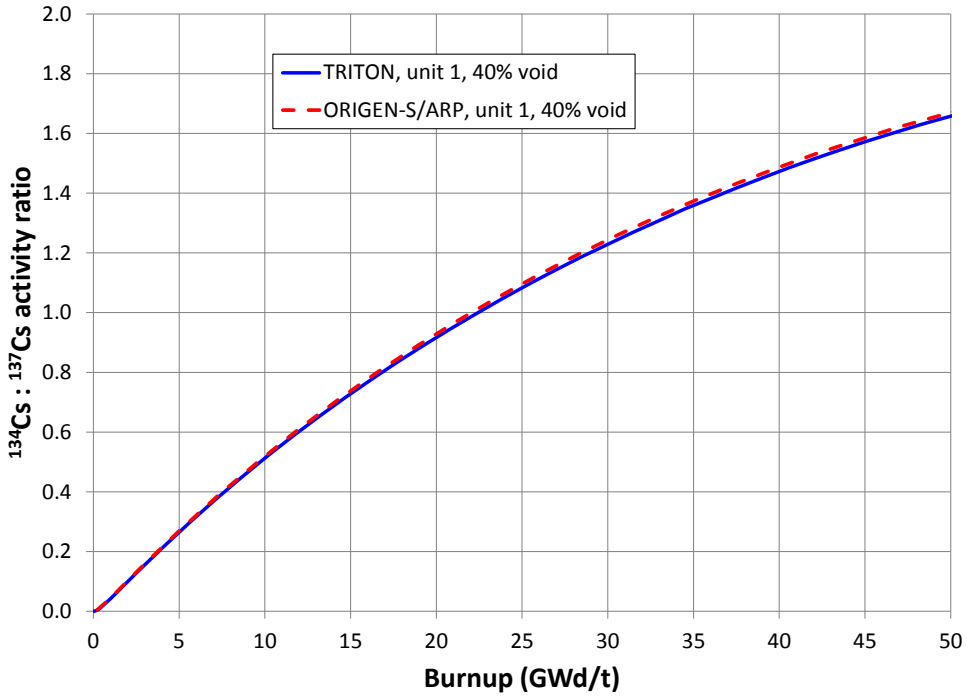

Figure 2.10. TRITON and standalone ORIGEN-S predictions of ^{134}Cs:^{137}Cs ratio for unit 1.

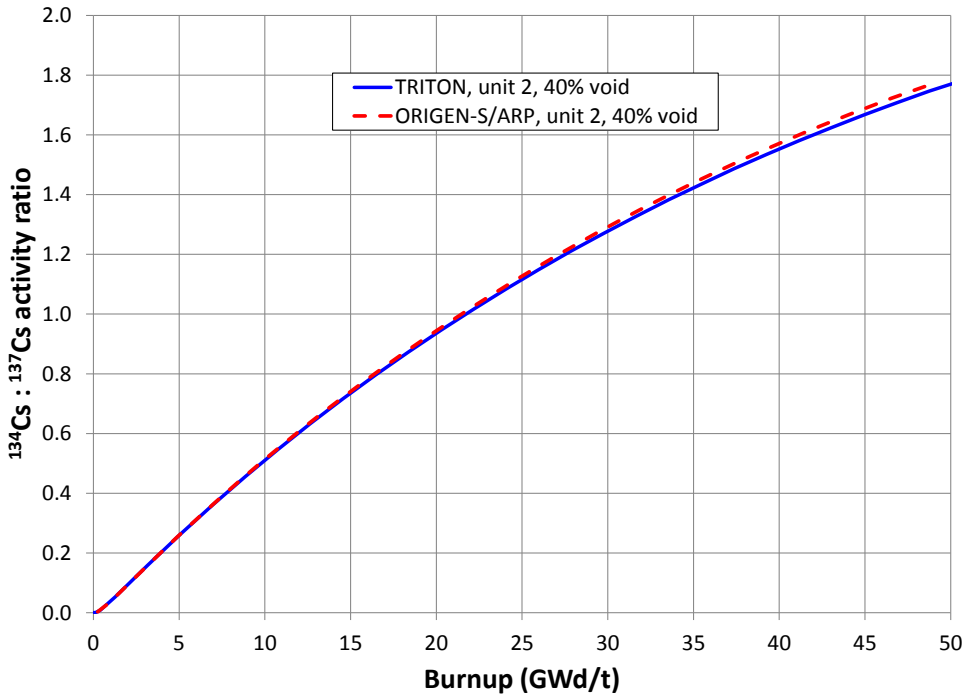

Figure 2.11. TRITON and standalone ORIGEN-S predictions of ^{134}Cs:^{137}Cs ratio for unit 2.

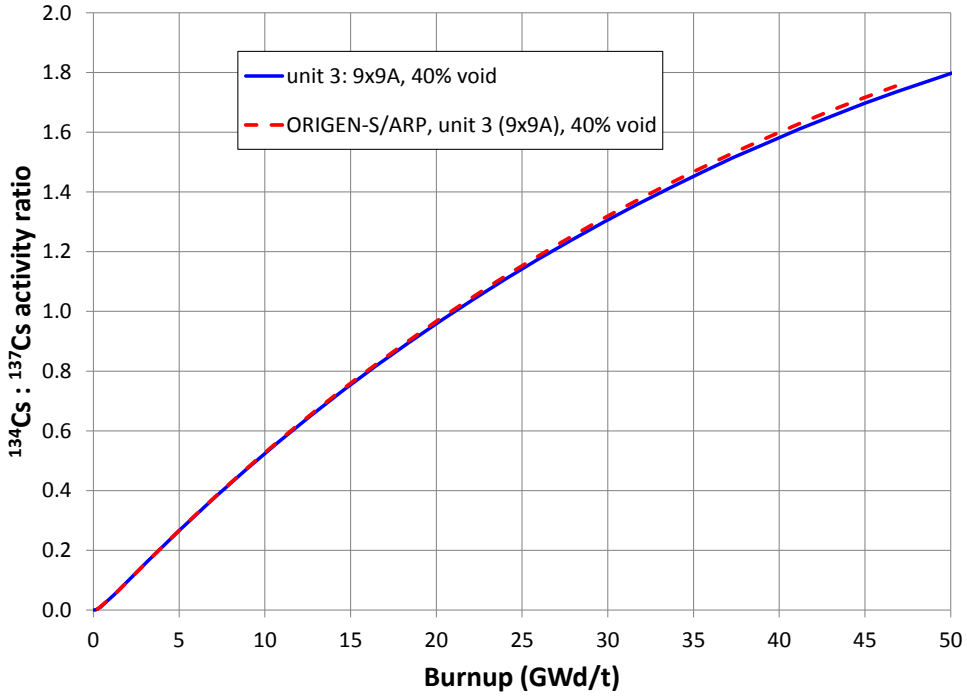

Figure 2.12. TRITON and standalone ORIGEN-S predictions of ^{134}Cs:^{137}Cs ratio for unit 3.

Figure 2.13 and Figure 2.14 show the variability of the ^{134}Cs:^{137}Cs ratio with respect to burnup, data library, and void fraction. Figure 2.14 focuses on burnup values near the Fukushima core averages. The curves represent distinct ORIGEN-S calculations for a 9x9 BWR assembly with a specific power level of 25.6 MW/t and a ^{235}U enrichment of 3.8 w/o. The blue curves reflect depletion calculations that use the pre-generated SCALE6 library for 9x9 BWR fuel ("atrium9-9"), which is based on ENDF/B-V cross section data [2.6]. The green and red curves use ENDF/B-VII-based libraries for the 9x9 assemblies in unit 2 and unit 3, respectively, which were generated for this work using TRITON (see Section 2.1). The dotted curves are calculations at 0% void; solid curves are at 40% void, which is a reasonable whole-core value; and dashed curves are at 80% void fraction.

Figure 2.13 and Figure 2.14 demonstrate how the ratio increases with burnup and high void fraction. The ratio initially starts near zero since the production of ^{134}Cs, an activation product of ^{133}Cs, initially lags that of ^{137}Cs, a direct fission product with high yield. As ^{134}Cs accumulates with neutron absorptions in ^{133}Cs, the ratio increases and eventually exceed 1.0 owing to the higher decay constant of ^{134}Cs – i.e. it decays faster than ^{137}Cs and thus has greater activity. Increased void fraction results in a harder spectrum and increased resonance absorption in ^{133}Cs. This process is modeled in the standalone ORIGEN-S calculations via the problem-dependent, one-group cross sections that were calculated by TRITON. The input coolant density allows ARP to automatically select and/or interpolate the appropriate cross section values for ORIGEN-S; similar interpolations are performed as necessary for enrichment and burnup.

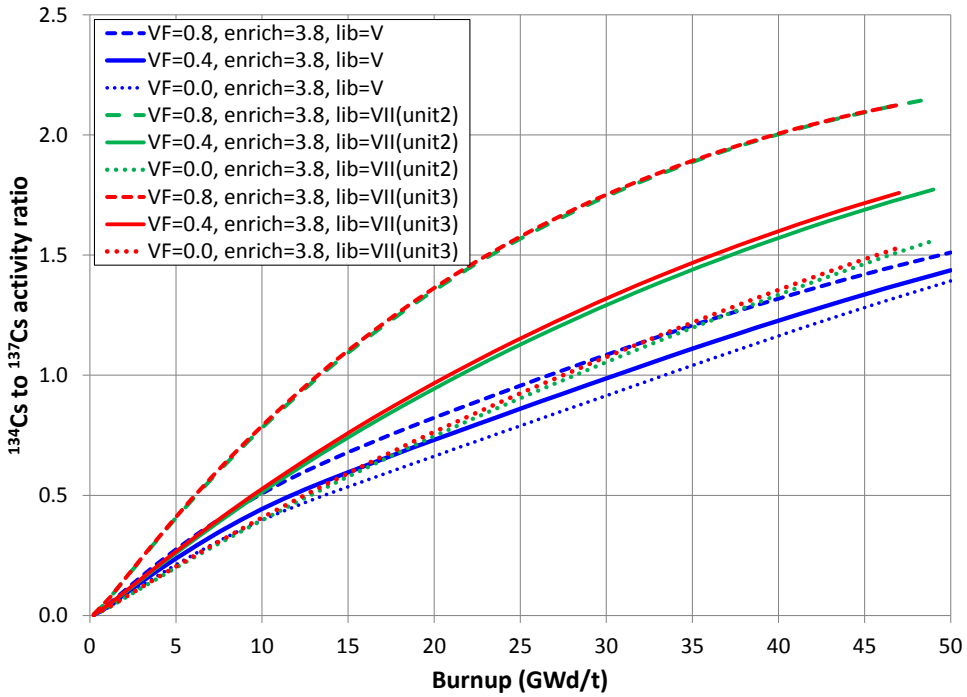

Figure 2.13. ^{134}Cs:^{137}Cs ratio for various library and void fraction (0 – 50 GWd/t).

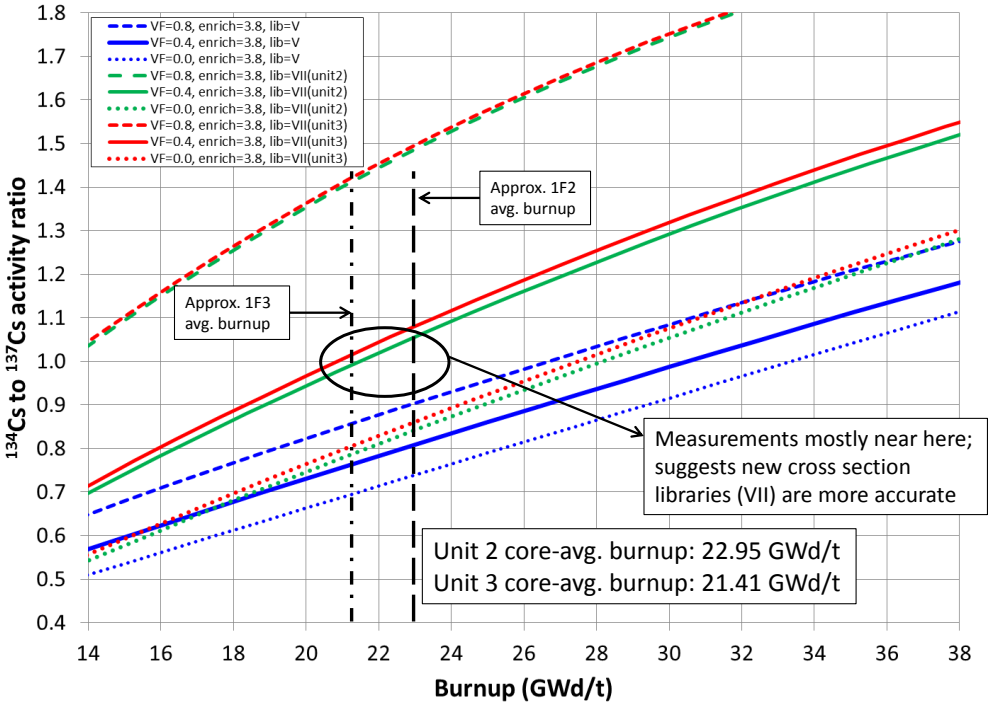

Figure 2.14. ^{134}Cs:^{137}Cs ratio for various library and void fraction.

Figure 2.13 and Figure 2.14 reveal a considerable discrepancy between the older ENDF/B-V libraries and the Fukushima-specific libraries that are based on ENDF/B-VII. In particular, the ENDF/B-V-based analyses under-predict the ^{134}Cs to ^{137}Cs activity ratio by about 20%, mainly due to reduced quantities of ^{134}Cs; the calculated ^{137}Cs inventory is acceptable. The average ratio at shutdown for each unit is reasonably well-known based on activity measurements outside the plant and several independent burnup analyses (see Section 2.2.3). Figure 2.14 shows that the ENDF/B-V-based calculations predict too low of a ratio relative to the ENDF/B-VII predictions for burnup values near the unit 2 and unit 3 average burnups–both of these units used 9x9 type assemblies. The solid red and green curves demonstrate that the slight geometric differences between the unit 2 9x9 (9x9B/STEP3B) and the unit 3 9x9 (9x9A/STEP3A) produce a 3-5% change in the predicted ratio; this is a relatively small change, but it may be significant to consider in source term analyses that use activity ratios for forensic insight. Most activity measurements at the plant yielded an average activity ratio near 1.0, as demarked by the circle on Figure 2.14. However, the activity measurements exhibit significant spread that might reflect the burnup spectrums in each core. This matter is investigated in Section 2.3.3.

These calculations suggest that the nuclear data libraries are important for accurate evaluation of key nuclide ratios. This would notionally include differences in fission yields and decay constants of pertinent nuclides, such as the yield of ^{133}Cs, but the capture cross section of ^{133}Cs is likely the more important quantity here. ^{134}Cs is not a (significant) direct fission product or decay product (^{134}Xe is stable), and thus ^{134}Cs is produced almost entirely from neutron absorption in ^{133}Cs, which is a high yield and stable fission product–hence it accumulates to large quantities. The ENDF/B-V-based library used in Figure 2.13 and Figure 2.14 is also based on a lattice geometry that does not match the Fukushima geometries, which influences the spatial and spectrum flux characteristics. Still, inspection of the continuous energy cross section data for

^{133}Cs reveals visually-distinguishable differences between ENDF/B-V and ENDF/B-VII data, thereby suggesting that the raw nuclear data is responsible for some of the calculation differences. The total neutron absorption cross section for ^{133}Cs is depicted in Figure 2.15. It illustrates that there is a visually-significant difference between the old (ENDF/B-V) and modern (ENDF/B-VII) nuclear data, particularly for the resonances above 10^{-4} MeV.

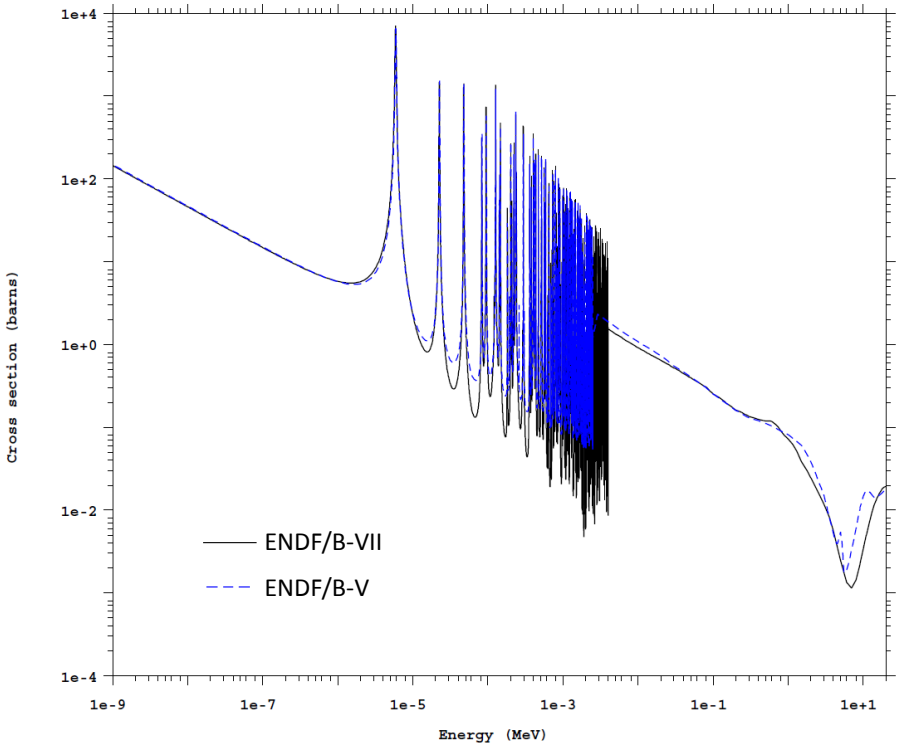

Figure 2.15. ^{133}Cs total absorption cross section.

2.3.2 Influence of Power Level and Previous Decay Periods

Integral burnup and nuclear data are the most dominant variables impacting the relative build-up of ^{134}Cs and ^{137}Cs. However, specific power level and decay periods during refueling also influence the ratio, albeit less significantly than overall burnup and cross section effects (namely void fraction). Higher power level – including both local power distribution and overall core power rating – is associated with greater activity ratio. Previously irradiated fuel also experiences variable length decay periods corresponding with the plant shutdown and refueling time. If the down town is rather long (e.g. over 30 days), the ratio can decrease due to ^{134}Cs decay; ^{134}Cs decays about 14 times faster than ^{137}Cs.

Figure 2.16 compares the cesium activity ratio for a 9x9 BWR assembly as a function of burnup and for two specific power levels: 20.3 MW/t and 25.6 MW/t given by the blue and red curves, respectively. The red and blue curves do not simulate any shutdown times. After about 15-20 GWd/t of burnup, the higher power case exhibits a significantly higher (~10%) cesium ratio. Thus fuel at identical burnup may have different ratios depending upon the rate of burnup. This

is one explanation for unit 1's lower overall ratio compared to units 2 and 3. Figure 2.16 also shows the influence of decay time during two hypothetical refueling outages that are assumed to last 180 days. This is evident by the lighter-blue dashed curve and its ratio discontinuities near 23 GWd/t and 46 GWd/t. No effective burnup is accrued during shutdown and the refueling outage manifests itself as a sudden drop in ratio. During this downtime, ^{134}Cs decays faster than ^{137}Cs and the activity ratio decreases. The ratio continues increasing once operation resumes. Based on these calculations, it appears that the most recent refueling outage is important for determining the activity ratio, and past outages may be of second-order significance. Shortly after operation resumes the ratio is 10-15% lower than the base case with no outages, but the ratio appears to 'catch up' to the base case as time into the current cycle increases. Unit 1 had recent shutdown periods that greatly exceeded those of unit 2 and unit 3; the past three refueling outages at unit 1 ranged from 180 days to 1080 days each. This is another explanation for the lower ratio exhibited by unit 1, despite its higher overall burnup. The long decay times for previously-irradiated fuel were implemented into the unit 1 calculations in this report (Section 2.2) in order to obtain a cesium ratio comparable to the BSAF values.

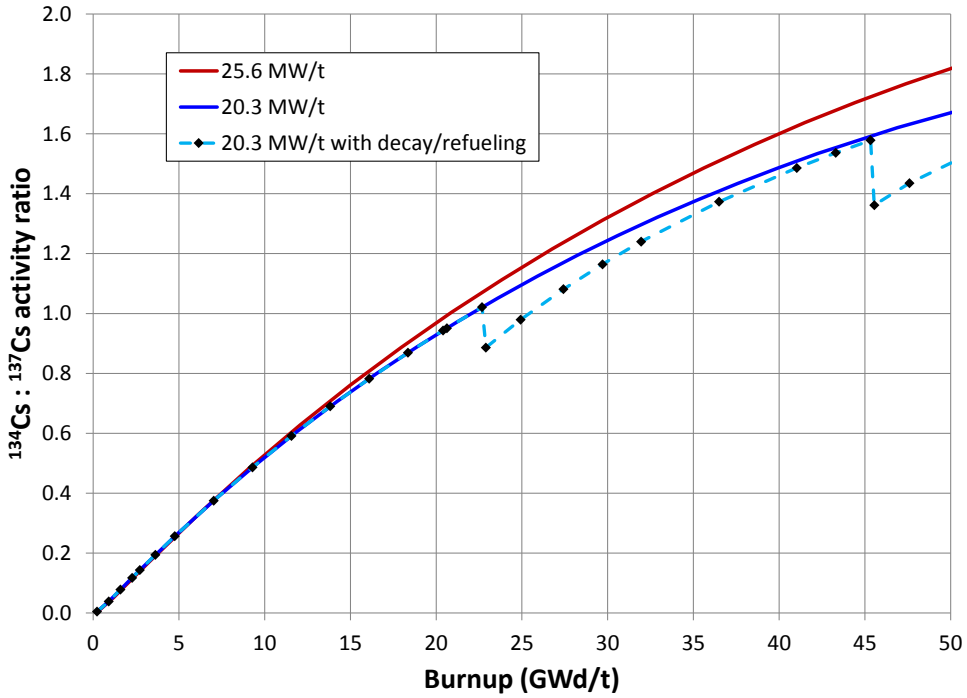

Figure 2.16. Ratio dependencies on power level and decay periods.

Figure 2.17 and Figure 2.18 demonstrate how ^{134}Cs:^{137}Cs ratio varies with decay time. Assuming an initial ratio of 1.0 (close to the whole-core Fukushima values), the ratio decreases linearly by less than 2% percent for 20 days of decay time, and about 16% after 200 days. The ratio is nearly a linear function for decay times significantly less than the half-life of ^{134}Cs (~2 years). For longer decay (Figure 2.18), the ratio starts to decrease more rapidly owing to ^{134}Cs decay. Figure 2.18 shows how important decay time can be for long outages like those at unit 1 – the ratio

could drop to half of its original value by the time reactor operation resumes, depending on the outage duration.

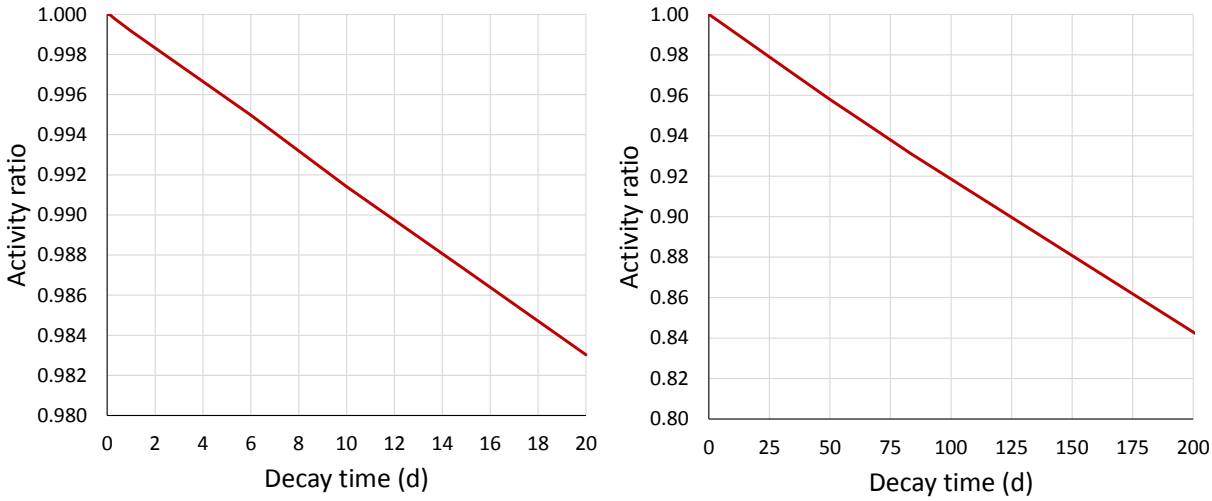

Figure 2.17. Cesium activity ratio as function of decay time (0-200 days).

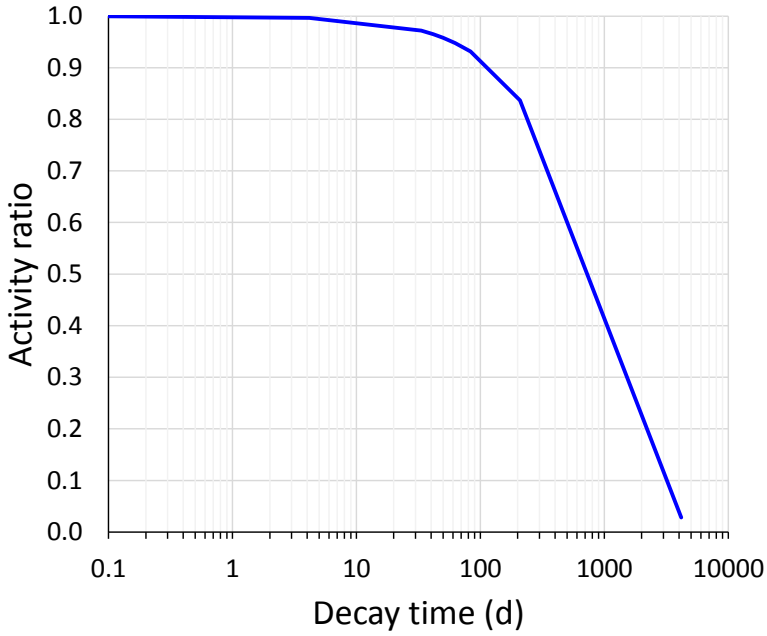

Figure 2.18. Cesium activity ratio for long decay time (0-11 years).

2.3.3 Distributions of ^{134}Cs to ^{137}Cs Activity Ratio

The burnup spectrum in a modern LWR core is highly heterogeneous. BWRs typically have 3-5 batches of fuel with different irradiation and decay histories, the batches being fresh fuel, once-irradiated fuel, twice-irradiated fuel, and so on. Therefore, schemes for reloading and shuffling of fuel assemblies create a range of burnups over the core. In the Fukushima reactors, assembly-averaged burnups at the time of last shutdown ranged from about 3 GWd/t to 42 GWd/t. The lowest burnup assemblies around 3-10 GWd/t were fresh fuel when initially loaded into the reactors.

Core burnup spectrums for units 1, 2, and 3 are shown by Figure 2.19, Figure 2.20, and Figure 2.21, respectfully. These figures show the calculated final (assembly-averaged) burnup distributions over each core, as predicted by ORIGEN-S. The left plot in each figure show histogram bin values in terms of number of assemblies over burnup bins with widths of 2 GWd/t, and the right plot shows the same information but the bin values are normalized to the total fuel assembly count in each core; unit 1 has 400 total assemblies, and units 2/3 have 548 assemblies. In each unit, at least four distinct fuel batches are evident, and the batches roughly comprise about one-quarter of the core each. The fresh fuel in each unit is readily apparent as the left-most cluster of assemblies in Figure 2.19, Figure 2.20, and Figure 2.21. A principal takeaway from these figures is that the burnup spectrums are not concentrated around the whole-core burnup values of 25.8 GWd/t, 22.95 GWd/t, and 21.4 GWd/t (for units 1, 2, and 3, respectively). In fact, unit 2 and unit 3 contain very few (if any) assemblies at their whole-core burnups. One of the fuel batches in unit 1 is centered near its whole-core burnup. The batches tend to overlap more as burnup increase, indicating slightly variable differential burnups in each batch, owing to assembly-specific power fraction in each cycle and fuel shuffling schemes.

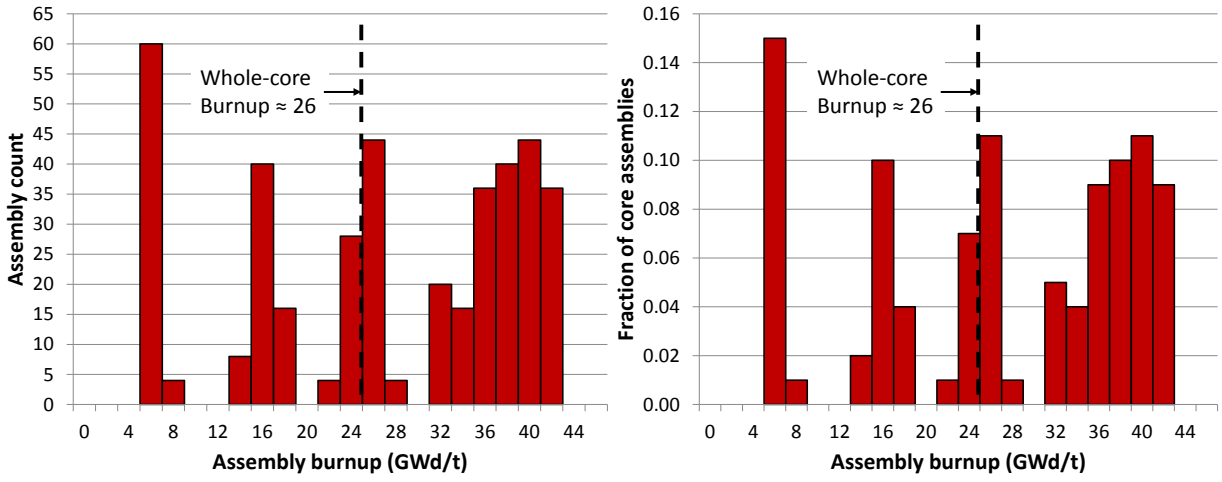

Figure 2.19. Unit 1 assembly-averaged burnup spectrum.

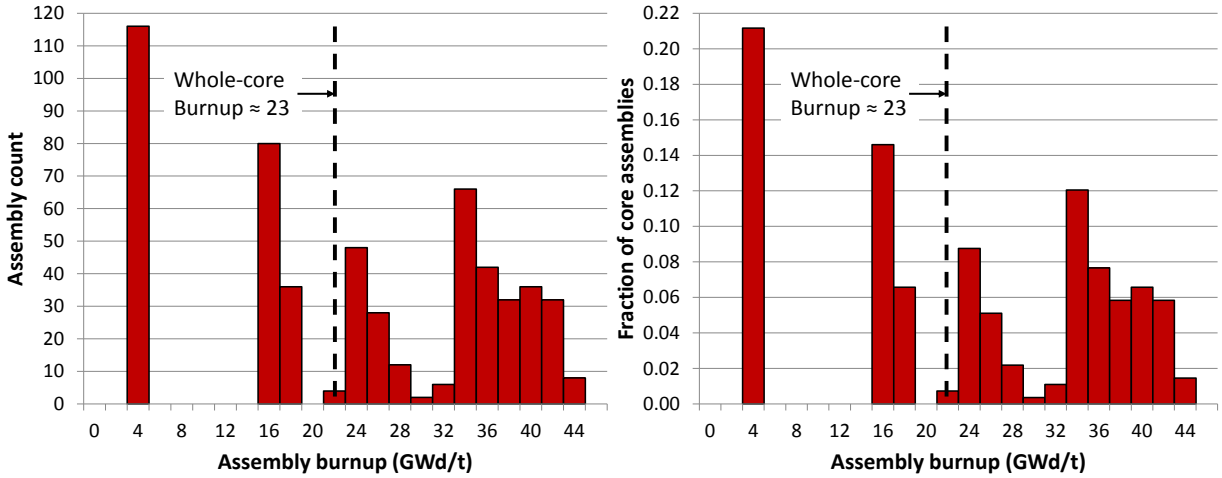

Figure 2.20. Unit 2 assembly-averaged burnup spectrum.

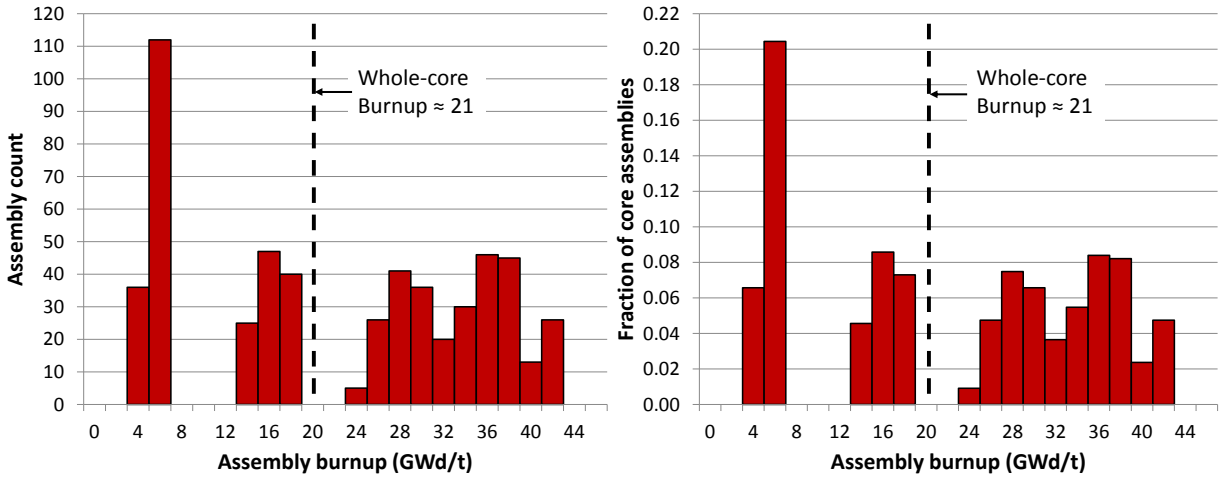

Figure 2.21. Unit 3 assembly-averaged burnup spectrum.

Because burnup is one of the key variables affecting the activity ratio of ^{134}Cs to ^{137}Cs, assembly histograms of the ratio should produce a similar distribution for each core. Figure 2.22, Figure 2.23, and Figure 2.24 portray the calculated activity ratio distributions for unit 1, unit 2, and unit 3, respectively. The ratio distributions are quite similar to the burnup distributions of each unit, but more bin overlap occurs across the distinct fuel batches due to other influences on the ratio, such as local/assembly power level. The spatial power distributions over the cores are probably the second-most dominant factor affecting the ratio in these analyses. Notionally the void fraction distribution, both axially and radially, would also be very important, but the ORIGEN-S analyses currently assumed identical void fractions for all assemblies and neglect axial variations in void and power level.

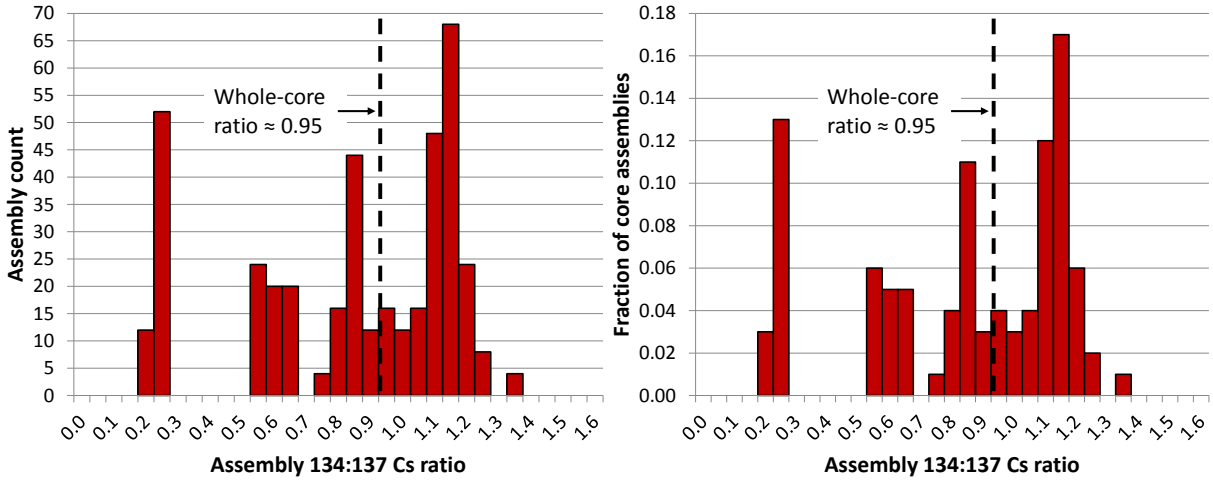

Figure 2.22. Assembly-averaged cesium activity ratio for unit 1.

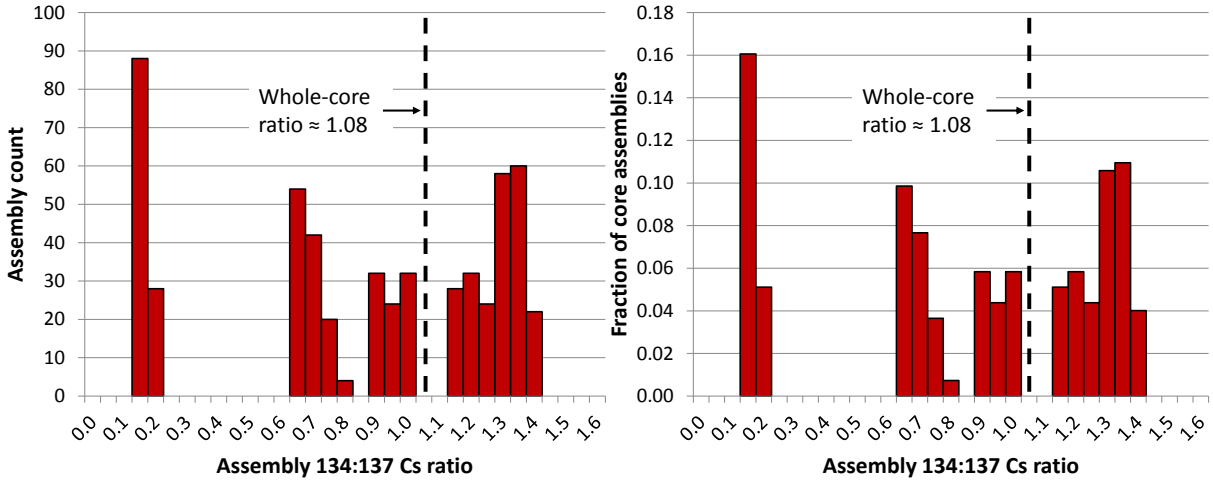

Figure 2.23. Assembly-averaged cesium activity ratio for unit 2.

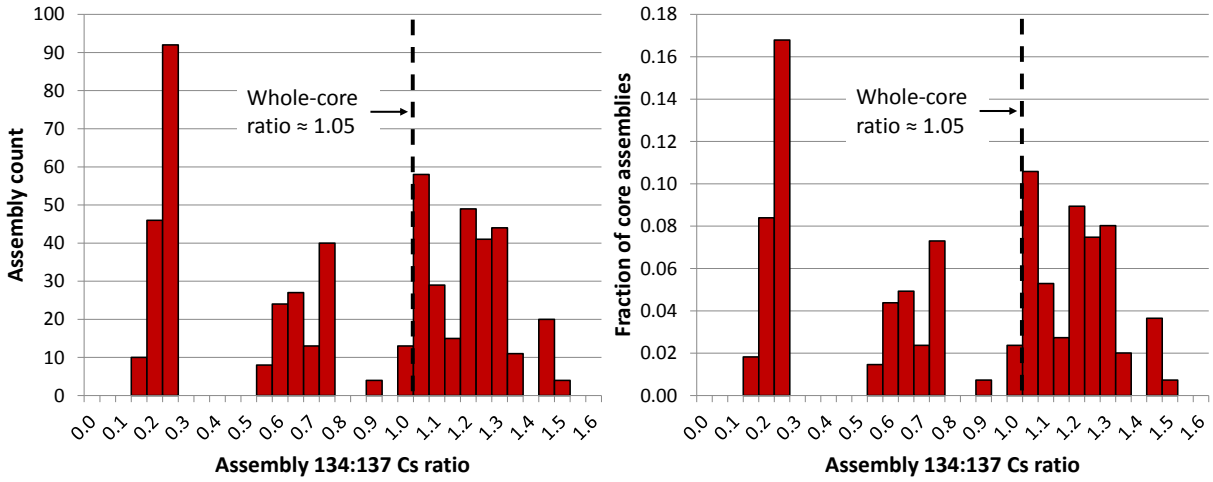

Figure 2.24. Assembly-averaged cesium activity ratio for unit 3.

Like the burnup distributions, the histograms of activity ratio are not centered nor concentrated around the whole-core values–they do not resemble a normal distribution. Unit 2 is actually predicted to have zero assemblies with activity ratio at its whole-core value. A key conclusion is established that the Fukushima cores did not have a single ^{134}Cs:^{137}Cs activity ratio, but instead have complex distributions of ratios that reflect the reactor's operating history, burnup and power distributions, thermal-hydraulic features (i.e. coolant density), lattice geometry, and fuel materials properties (e.g. enrichment and MOX).

When the activity ratio information is mapped over the core, the spatial distribution of the ratio clearly reflects the burnup distribution. Figure 2.25 and Figure 2.26 show the 2D spatial distribution of the ratio for unit 3. In Figure 2.25, red assemblies reflect regions of high ^{134}Cs to ^{137}Cs ratio; high ratio value is also illustrated by the z-elevation of the assemblies. The flat, dark blue regions are outside the active core region. The light blue assemblies denote ratios around 0.1 to 0.3; these assemblies are a bit obscured by the 3D facets in Figure 2.25, and Figure 2.26 better illustrates the heterogeneous check-boarding of high and low assembly ratios throughout the inner core. The outer core ring is comprised entirely of high ratio assemblies due to the shuffling of high burnup fuel from previous cycles to the core periphery.

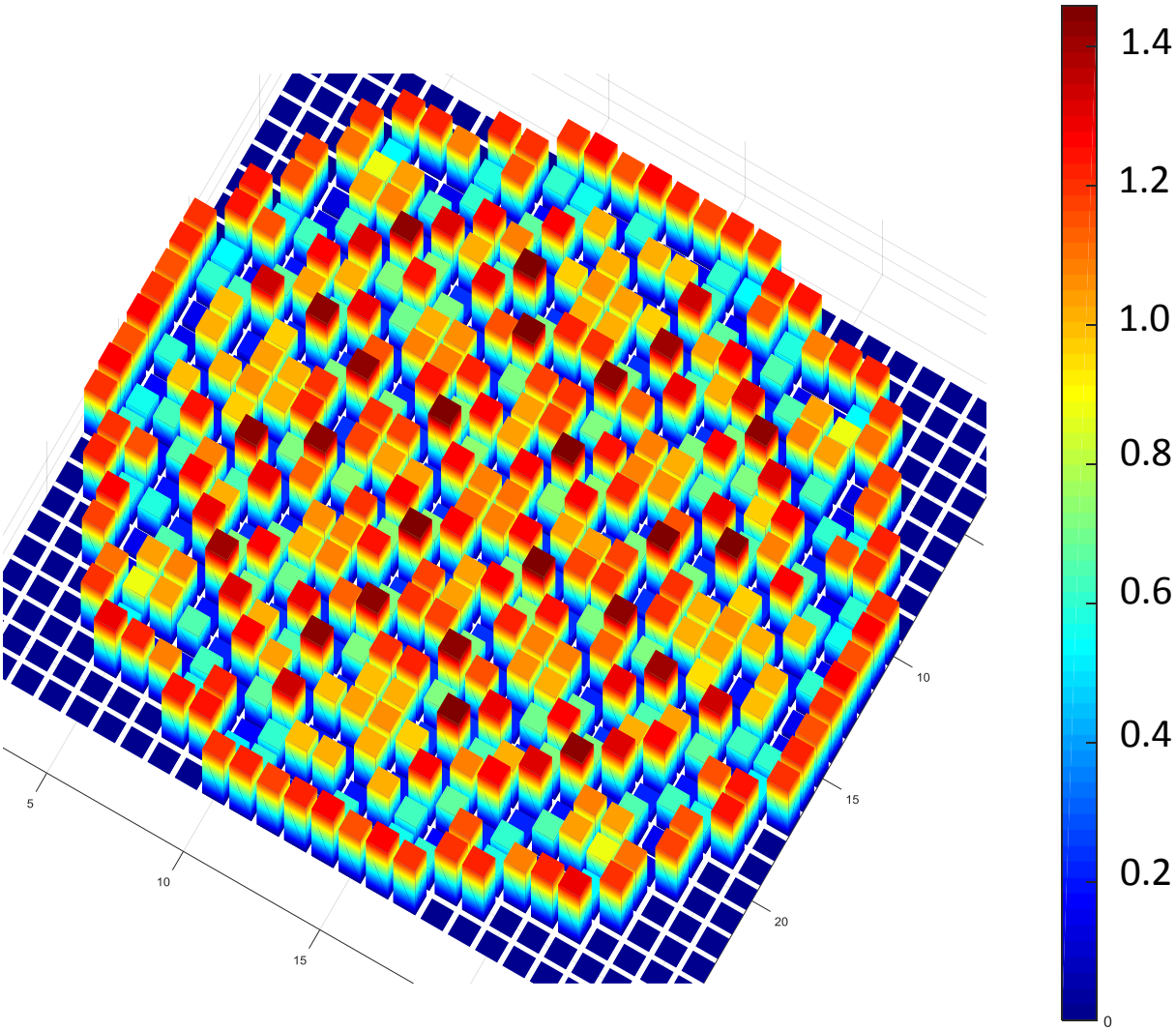

Figure 2.25. 2D spatial distribution of ^{134}Cs:^{137}Cs activity ratio.

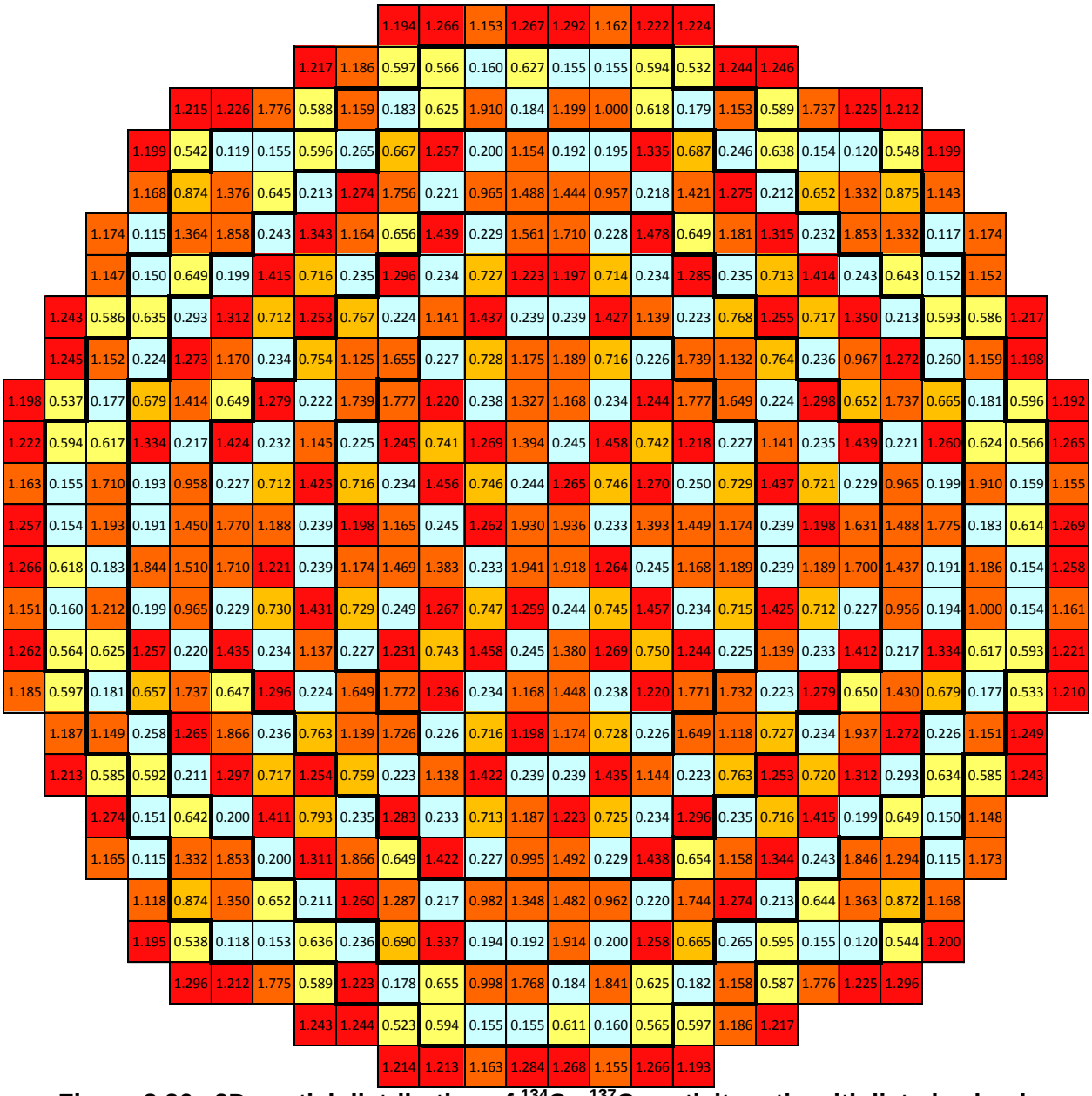

Figure 2.26. 2D spatial distribution of ^{134}Cs:^{137}Cs activity ratio with listed valued.

Another fundamental aspect of the ratio distribution is the fact that the simple mean value of several ratios, such as over each assembly or for several measurements, may not be the best measure of the whole-core ratio. For instance, the whole core ratio from the BSAF and SNL analyses (Table 2-16) is defined by the formula below, where A is the local ^{134}Cs activity, B is the local ^{137}Cs activity, the index (i) is for each fuel assembly (or each measurement), and N denotes the total number of assemblies (or total number of measurements):

$$whole\ core\ ratio = \frac{\sum_i^N A_i}{\sum_i^N B_i}$$

This quantity is just the ratio of the *whole-core inventories* of ^{134}Cs and ^{137}Cs. Naturally, this is not equivalent to the average value of several individual ratios since the denominators of each ratio (i.e. the ^{137}Cs inventory) are not the same. The mean value of several ratios is simply the sum of the ratios divided by the total number of ratio values, which corresponds to the number of assemblies (or perhaps a number of different measurements). Stated mathematically below, the actual whole-core ratio is not equal to the sum of individual ratios divided by the total number:

$$\frac{\sum_i^N A_i}{\sum_i^N B_i} \neq \frac{1}{N}\sum_i^N \left(\frac{A}{B}\right)_i$$

Or,

$$\frac{A_1 + A_2 + A_3 + \cdots A_N}{B_1 + B_2 + B_3 + \cdots B_N} \neq \frac{1}{N}\left(\frac{A_1}{B_1} + \frac{A_2}{B_2} + \frac{A_3}{B_3} + \cdots \frac{A_N}{B_N}\right)$$

It is for this reason that taking the simple average of the ratios shown in Figure 2.24 and Figure 2.26 will not yield the real whole-core ratio for unit 3 listed in Table 2-16. For similar reasons, care should be taken when comparing ratios measured outside the reactors to the initial core values predicted by burnup codes; averaging several measured ratios might produce an invalid or misleading point estimate. The introduced error might be small, but the whole-core burnups and ratios are close enough that it may still be significant. A better approach may be to divide the average measured cesium ^{134}Cs activity density by the average measure ^{137}Cs activity density at each location.

Concerning the measured activities around the plant, the cesium ratio exhibits a spread of roughly 0.6 to 1.2 for most data points soon after the accident [2.5][2.9]. Judging by the calculated distributions of cesium ratio, the range of measured ratios appears to be representative of the burnup distributions in each core. A low measurement around 0.6 is very reasonable, since many assemblies in each core have burnups that yield such a ratio (Figure 2.22, Figure 2.23, Figure 2.24); likewise, measurements of 1.2 are not surprising given the core burnup distributions and associated cesium ratios. Therefore, the range of measured ratios may not be exclusively due to measurement uncertainty–it may simply reflect the core burnup spectrums.

There is evidence that cesium from the cores was mixed and somewhat homogenized after release from fuel and subsequent transport to the environment. The distribution of measured ratio starts to resemble a normal distribution [2.9], which is in contrast to the more-complicated initial core distributions. To some extent, this is to be expected since many fuel assemblies in the core likely release cesium around the time, after which the cesium from separate assemblies (with unique burnups) mixes and transports identically no matter the nuclide composition; all cesium is believed to behave chemically and physically the same (or nearly so) for radionuclide transport independent of nuclear properties. That said, there may be distinct periods of cesium release from the cores such as gap releases from the hottest assemblies (most likely once-burned fuel in the central core [2.2]) that have lower burnups/ratios, and delayed releases from cooler outer core assemblies with higher burnups/ratios. Note that the power distributions are largely center-peaked in each core, while the spatial burnup distribution is nearly an inverse shape [2.4]. Delayed cesium releases might also occur if the corium escaped ex-vessel after RPV lower head failure. Ex-vessel cesium releases could largely emanate from high burnup assemblies with

higher ^{134}Cs:^{137}Cs ratio. At this point in the accident, the lower burnup assemblies from the inner core would have likely already released most of their cesium inventories.

2.3.4 Code Comparison of ^{134}Cs to ^{137}Cs Ratio

A code comparison is conducted to further gauge the sensitivities of the cesium ratio as predicted by depletion codes using modern nuclear data. MCNP6 burnup calculations are compared to those of ORIGEN-S. The standalone ORIGEN-S predictions of cesium ratio were markedly similar to values obtained directly out of TRITON; thus the figures in this section are also an effective comparison of MCNP6 and TRITON.

An MCNP6 geometry model of BWR fuel assembly is created that is comparable to the 9x9B (STEP3B) assembly that was used in units 1 and 2. There are some small geometric differences between the MCNP6 model and the TRITON geometry that generated the data libraries for ORIGEN-S, such as the corners on the channel box and water rod being approximated as right angles instead of rounded. Such approximations are implemented to expedite a scoping comparison between MCNP6 and the SCALE6 tools–hence this is not a rigorous benchmark comparison, but is rather intended to highlight that the codes produce similar trends. Because Monte-Carlo burnup calculations are relatively CPU-intensive, requiring sufficiently-resolved statistics of several reaction tallies for each nuclide being tracked, only a few MCNP6 depletion analyses are completed for this work. The MCNP6 calculations were executed using 400-600 cores on SNL's supercomputing resources.

The cesium ratios calculated using ORIGEN-S and MCNP6 are qualitatively similar, as evident by Figure 2.27. Both codes predict the ratio starting near zero and increasing to a value near 1.0 after 20 GWd/t of burnup. As burnup increases further, the ratio begins to gradually roll over as the ^{134}Cs activity approaches its equilibrium value, which occurs sooner than that of ^{137}Cs (its inventory still increases for some time). Around the average burnups of units 2 and 3 (21-23 GWd/t), the MCNP6 ratio is about 6% lower than the ORIGEN-S calculation for the unit 2 fuel assembly. This is only a cursory demonstration of the precision of modern burnup codes in determining ^{134}Cs:^{137}Cs ratio, but it provides some guidance in assigning point-estimate values of the ratio for each unit for comparison to measurement data of cesium deposition.

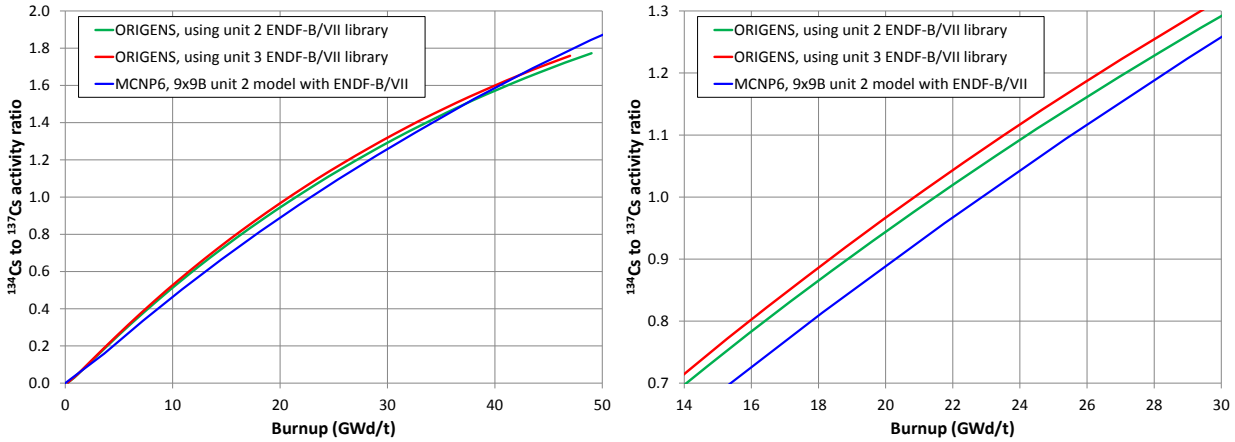

Figure 2.27. ORIGEN-S and MCNP6 predictions of cesium activity ratio.

2.4 Section 2 References

[2.1] TEPCO Plant Data, http://www.tepco.co.jp/nu/fukushima-np/plant-data/f1_3_Keihou3.pdf, accessed August 16 (2016).

[2.2] T. Endo, et al, "Estimation of the average burnup of damaged fuel loaded in Fukushima Daiichi Reactors by using the $^{134}Cs/^{137}Cs$ ratio method," Nagoya University, 2011 Symposium on Nuclear Data, Nov. 17th (2011).

[2.3] K. Nishihara, et al., "Estimation of Fuel Compositions in Fukushima-Daiichi Nuclear Power Plant," 2012-018, Japan Atomic Energy Agency (2012). Available at http://jolissrch-inter.tokai-sc.jaea.go.jp/pdfdata/JAEA-Data-Code-2012-018.pdf

[2.4] J.N. Cardoni, "Radionuclide Inventory and Decay Heat Quantification Methodology for Severe Accident Simulations," SAND2014-3966 (OUO Report), Sandia National Laboratories, Albuquerque, NM (2014).

[2.5] BSAF, Information Portal for the Fukushima Daiichi Accident Analysis and Decommissioning Activities, https://fdada.info/en/.

[2.6] Oak Ridge National Laboratory, "Scale: A Comprehensive Modeling and Simulation Suite for Nuclear Safety Analysis and Design," ORNL/TM-2005/39, Version 6.1, June 2011. Available from Radiation Safety Information Computational Center at Oak Ridge National Laboratory as CCC-785.

[2.7] B. J. Ade, NUREG/CR-7041, "SCALE/TRITON Primer: A Primer for Light Water Reactor Lattice Physics Calculations," ORNL/TM-2011/21, Oak Ridge National Laboratory, Oak Ridge, TN (2012).

[2.8] K. Okumura, et al., "SRAC2006: A Comprehensive Neutronics Calculation Code System," JAEA-Data/Code 2007-004, Japan Atomic Energy Agency, 4-49 Muramatsu, Tokai-mura, Naka-gun, Ibaraki 319-1184, Japan (2007).

[2.9] B.S. Jackel, et al., "Land contamination activity data interpretation from Fukushima Daiichi Accident," Nuclear Engineering and Design, 300, pp. 28-33 (2016).

3 SUMMARY AND CONCLUSIONS

Radionuclide inventories for the damaged Fukushima Daiichi reactors have been generated for use in subsequent severe accident research. The calculated inventories were found to compare reasonably well with international analyses for the BSAF project. Some high-level conclusions and future work are discussed in this section.

3.1 High Level Conclusions

SCALE6 analyses have been conducted to generate isotopic-level radionuclide inventories to support Phase II of BSAF. The burnup simulations implemented Fukushima-specific cross section data derived from TRITON analyses of the Fukushima fuel. Accurate radionuclide inventories are required information for best-estimate severe accident calculations, dose calculations, and source term and consequence analyses.

The predicted inventories compare well with JAEA-calculated values. Most importantly, predicted activities of key nuclides such as ^{131}I, ^{134}Cs, and ^{137}Cs are very similar between the SNL and JAEA analyses. Both sets of inventory information are acceptable for best-estimate analyses of the Fukushima reactors. If other BSAF members implement the JAEA inventory, it is probably advisable to do likewise in order to facilitate code comparison. However, implementation of alternative inventories is also recommended to increase the technical confidence in source term analyses. Use of different inventories may corroborate the JAEA information and/or highlight areas for improvement. Multiple burnup calculations also yield insights into the sensitivities of certain nuclide quantities like ^{134}Cs and several actinides. Such rigorous efforts therefore provide a technical basis for defining point-estimates (or uncertainty bounds) of the nuclear characteristics of each unit, and this information is of fundamental utility for accident forensics, reactor decommissioning, and expanding the state-of-knowledge of severe accidents.

Depletion and decay calculations for ^{134}Cs to ^{137}Cs activity ratio were explored using SCALE6 and MCNP6. Overall burnup and nuclear data are found to be of primary significance in determining the cesium ratio. Cesium ratio generally increases as a function of burnup, starting near zero and approaching 1.0 around 20 GWd/t, and then gradually rolls over as burnup increases due to ^{134}Cs approaching its equilibrium activity; ^{134}Cs has a 2 year half-live in comparison to the ~30 year half-live of ^{137}Cs. The one-group cross sections provided to the depletion code have a strong impact on the predicted ^{134}Cs activity, since this nuclide accumulates due to neutron absorption in ^{133}Cs. The base data library (e.g. ENDF/B-V vs. ENDF/B-VII) used in lattice calculations is important, as is the assumed void fraction of the coolant/moderator. Higher void fraction leads to a harder neutron spectrum and increased resonance absorption in ^{133}Cs, and hence the cesium ratio increases. Finally, burnup/decay calculations with various power level and decay time revealed some interesting dependencies that explain the lower cesium ratio of unit 1 – unit 1 had the greatest burnup (in GWd/t) but lower power level than the other units. Plus, it had several extended shutdown periods that involved decay time on the order of years. Lower power level and longer previous decay periods contribute to decreased cesium ratio.

Analyses of cesium ratio investigated the direct effects of the highly heterogeneous burnup distributions in each core. Batches of fuel assemblies tend to have comparable burnup, and this leads to distinct clusters of cesium ratio over the cores. It is found that the Fukushima units do not exhibit a normal distribution of ^{134}Cs:^{137}Cs activity ratio. Instead, the cesium ratio over each core is a complicated distribution that mostly follows the burnup profile. Thus, assigning point-values for each unit may involve additional challenges for comparing to measured deposition data. Specifically, it is unknown how the cesium was released from each core and how the cesium may have mixed with assemblies of different burnup or even with cesium from the other units. Cesium releases from the inner core, where decay heat is greater but average burnup is lower, would exhibit lower cesium ratio; conversely, outer core assemblies, where decay heat is lower but burnup is higher, would exhibit higher cesium ratio. The measured ratios have a spread that aligns itself with the predicted cesium ratios, which chiefly correspond with the burnup profiles of the cores. However, mixing of different cesium (i.e. with unique isotopic compositions) is evident in the data, and several of the measured values were at the detection limit and thus may be unreliable. Ultimately, the whole-core cesium ratios of each unit are quite similar (as predicted by burnup analyses), mainly since the gross burnups were comparable. Rigorous statistical methods that account for the burnup and ratio spectrums of the cores may be useful in associating measured data to a specific unit.

3.2 Future Work

Near term future efforts will focus on utilizing the calculated radionuclide inventories to support Phase 2 of BSAF. This includes severe accident simulations out to 3 weeks using MELCOR, plant dose analyses using MCNP, and dispersion and consequence calculations using MACCS. All of these analyses will be compared to plant data of event timing, pressure, water level, dose rate, and radionuclide deposition (measured activities).

Long-term future work potentially includes:

- **Improved accounting of 3D (mainly axial) effects on the inventory of important neutron absorption products such as ^{134}Cs.**
  The influences on axial void fraction and local absorption reaction rates in ^{133}Cs can be explored for various conditions.

- **Expanded modeling of previously irradiated fuel assemblies.**
  The current ORIGEN-S calculations explicitly simulate the details of the last operating cycle of each unit, but approximate the burnup of previously irradiated fuel. The number of previous irradiation cycles was assumed/inferred, the specific power levels were taken to be the core averages (which neglects power distribution in the previous cycles), and the treatment of decay downtimes between irradiation cycles was simplified. These approximations were necessary due to a lack in available plant information. However, additional plant information on each assembly's burnup history in units 1-3 has recently been made accessible for future BSAF work.

- **Derive severe accident information using coupled neutron transport and depletion calculations directly**.
  Severe accident inventories for the Fukushima cores in this report were mostly derived using standalone ORIGEN-S calculations. Although these calculations implement data libraries from coupled neutron transport and depletion models (TRITON), the TRITON simulations are capable of directly calculating the desired information. However, TRITON analyses on an assembly-level basis would require at least 1496 separate calculations (548 assemblies in units 2 and 3, 400 in unit 1); this incurs higher CPU costs, especially if sensitivity studies are necessary.

- **Corroborate BSAF and current depletion calculations using most recent, state-of-the-art nuclear analysis tools.**
  The depletion calculations in this work used TRITON, ORIGEN-S, and ARP in the SCALE6.1.3 code package. SCALE6.2 includes expanded features for calculating nuclear severe accident quantities, and it has updated ENDF/B-VII-based cross section libraries for standalone depletion analyses. Updated calculations using the latest SCALE release would provide another set of data to substantiate the BSAF information and the current calculations in this report, and this would increase the technical confidence in the radionuclide quantities for severe accident analyses.

Additional work should entail rigorous statistical assessment of radio-assay measurements that were taken in the spent fuel pools, turbine halls, and around the plants. Cesium activity ratio of ^{134}Cs and ^{137}Cs will of course be a major part of these efforts, but other nuclide ratios (particularly same-class nuclides) will also be explored. This data will be compared to deposition measurements especially for the large plume to the northwest of the plant. Another method of assessing unit-representative cesium ratios will involve analysis of gamma spectroscopy data that is available for cesium deposited below the shield plugs. Radionuclides deposited below the shield plugs should allow for the best determination of characteristic cesium ratios for each unit, since it was highly unlikely for external cesium to ingress below the shield plug. In collaboration with MELCOR and MACCS studies, nuclear analyses may yield novel insights on accident forensics and reactor decommissioning.

APPENDIX A: SEVERE ACCIDENT QUANTITIES

This work focused on evaluation of isotopic inventories for Fukushima Daiichi units 1-3 using ORIGEN-S. These same calculations can produce consistent sets of severe accident quantities such as gross RN class masses and decay heat curves. Generation of class quantities is basically a matter of element-based summation over the radionuclides, consistent with past severe accident methodology and MELCOR best practices [1]-[4]. This information is essential input for severe accident analyses using codes such as MELCOR.

Section A.1 summarizes the tabulated RN class masses for each unit. Section A.2 describes the decay heat as a function of time after shutdown. Decay power distributions over the cores are presented in Section A.3. RN masses and total decay power are compared to BSAF values calculated by JAEA.

Generally, the updated severe accident information is very similar to previous SNL calculations that also used ORIGEN-S but with less-representative, ENDF/B-V-based cross section libraries [5]. The use of Fukushima-specific data libraries is more significant for nuclide inventories, particularly for actinides and neutron absorption products. RN information for severe accidents is integral in nature (whole-core decay heat, lumped chemical/physical classes) and less sensitive to differences in cross section libraries. Nonetheless, it is expedient and logical to maintain consistent sets of radionuclide information for both isotopic and lumped-RN-class inventories.

A.1 Lumped RN Class Inventories

Table A-1 lists RN class mass inventories for use in MELCOR severe accident simulations. The lumped inventories are derived from the same ORIGEN-S calculations for the isotopic inventories. RN classes are predominately comprised of long-lived and stable nuclides by mass, and hence these values are less sensitive to modeling techniques and nuclear data. The most important variable for these quantities are overall reactor burnup and core size (i.e. gross fuel load). Unit 2 generally has the largest inventories due to its burnup compared to unit 3 and its larger size than unit 1, but unit 3 does possess slightly higher Tetravalent class mass (which includes plutonium) due to its MOX fuel. The RN class masses are only for nuclides residing in the fuel and do not include structural masses like the Zr in the Zircaloy cladding. Furthermore, oxygen in UO_2 is also not included in MELCOR–this mass is accounted for by sensitivity coefficients for the uranium class. Class masses for the volatile main groups (Cd and Ag) are sensitive to assumed impurities that may be initially present in the fuel. Similarly, the Trivalent class mass depends on the amount of burnable poison assumed/approximated for each assembly. This Gd (from Gd_2O_3) is mass that resides in the fuel and thus it notionally should be included in the RN class inventory.

Table A-1: Lumped RN inventories for Fukushima units 1-3.

#	Class (representative)	SNL-1F1 (kg)	SNL-1F2 (kg)	SNL-1F3 (kg)
1	Noble Gases (Xe)	301.65	371.14	346.76
2	Alkali Metals (Cs)	172.24	212.90	200.71
3	Alkaline Earths (Ba)	129.92	159.63	149.30
4	Halogens (I)	11.27	13.97	13.14
5	Chalcogens (Te)	28.09	34.52	32.32
6	Platinoids (Ru)	200.35	243.44	227.71
7	Early Transition Elements (Mo)	228.04	280.30	262.25
8	Tetravalent (Ce)	766.09	1005.93	1161.87
9	Trivalents (La)	640.84	812.17	777.98
10	Uranium (U)	65737.65	90323.99	91068.94
11	More Volatile Main Group (Cd)	7.18	9.15	8.75
12	Less Volatile Main Group (Ag/Sn)	6.40	7.73	7.31

The JAEA inventories include masses of stable nuclides that allows for summation of RN class inventories, and these can be compared to the SNL values. A rigorous review of this information has not yet been completed, but some pertinent class inventories for unit 1 are juxtaposed in Table A-2 below. These class masses are in excellent agreement excluding the halogen class with a 16.5% difference. Nevertheless, a less than 2 kg difference (13.13 kg – 11.27 kg) is probably of second order importance for most source term analyses. The difference appears to be mostly attributable to ^{129}I, the largest isotope in the class by mass, which is long-lived with a half-life of 1.57×10^{7} years. This could be indicative of different nuclear data for fission product yields and/or decay data.

Table A-2: Comparison of SNL and JAEA inventories of select RN classes.

Class (representative)	SNL-1F1 (kg)	JAEA-1F1 (kg)	% difference
Noble Gases (Xe)	301.65	300.90	0.25
Alkali Metals (Cs)	172.24	175.25	1.75
Alkaline Earths (Ba)	129.92	130.66	0.56
Halogens (I)	11.27	13.13	16.52
Chalcogens (Te)	28.09	28.57	1.69
Platinoids (Ru)	200.35	209.55	4.59

A.2 Decay Heat

Figure A.1 through Figure A.6 depict the decay power curves for Fukushima units 1-3 as a function of decay time after final shutdown. Each unit has separate plots of time plotted on a logarithmic time scale to 10^{7} s and on a severe accident time scale out to 300 hours. The SNL-calculated decay power curves are quantitatively similar to the JAEA values, as each respective curve is less than 7% different for all decay times. The largest discrepancy is immediately after

shutdown (less than 10 s) for each unit where the SNL and JAEA powers differ by 4-7%. However, the decay curves are within a few percent for most other decay times. The slightly divergence for early decay time is indicative of different predicted inventories of short-lived nuclides that drive decay power during this time period; this might be the result of different nuclear decay used in the analyses including fission yields, decay data, and cross sections. For example, the neutron absorption cross section of ^{238}U affects the production of ^{239}U and subsequently ^{239}Np (see Figure 2.9), both of which are important decay heat contributors shortly after reactor shutdown.

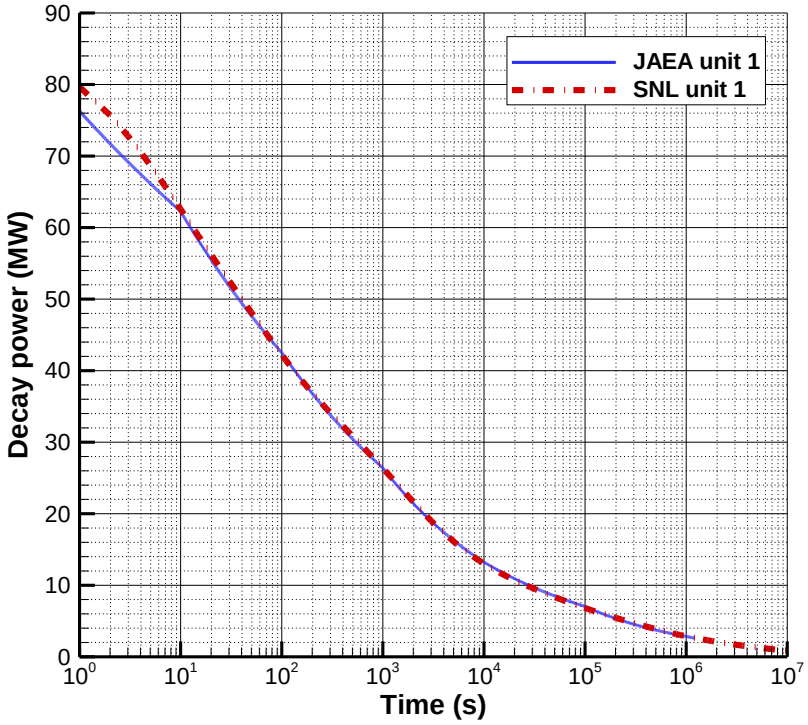

Figure A.1. Unit 1 decay power.

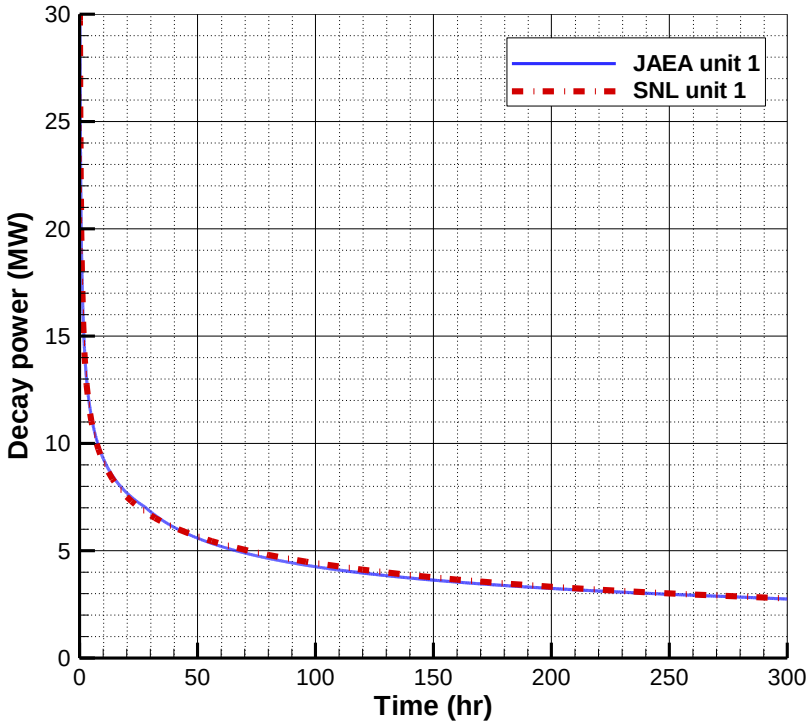

Figure A.2. Unit 1 decay power on severe accident time scale.

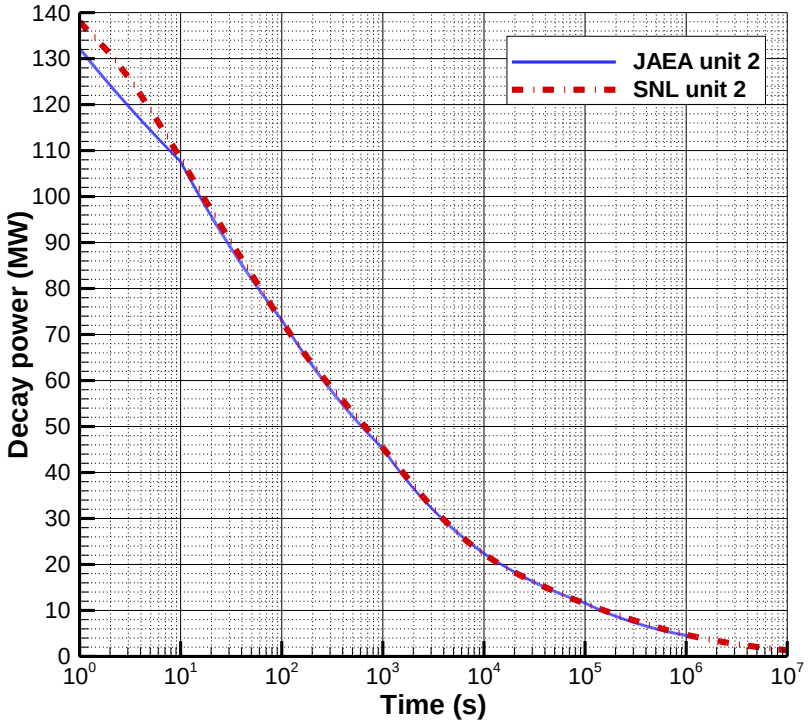

Figure A.3. Unit 2 decay power.

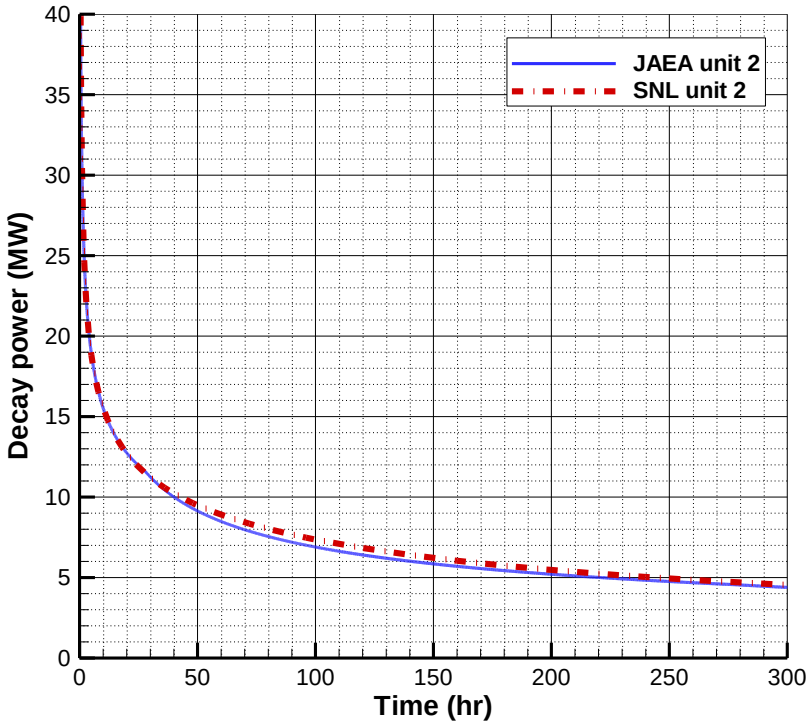

Figure A.4. Unit 2 decay power on severe accident time scale.

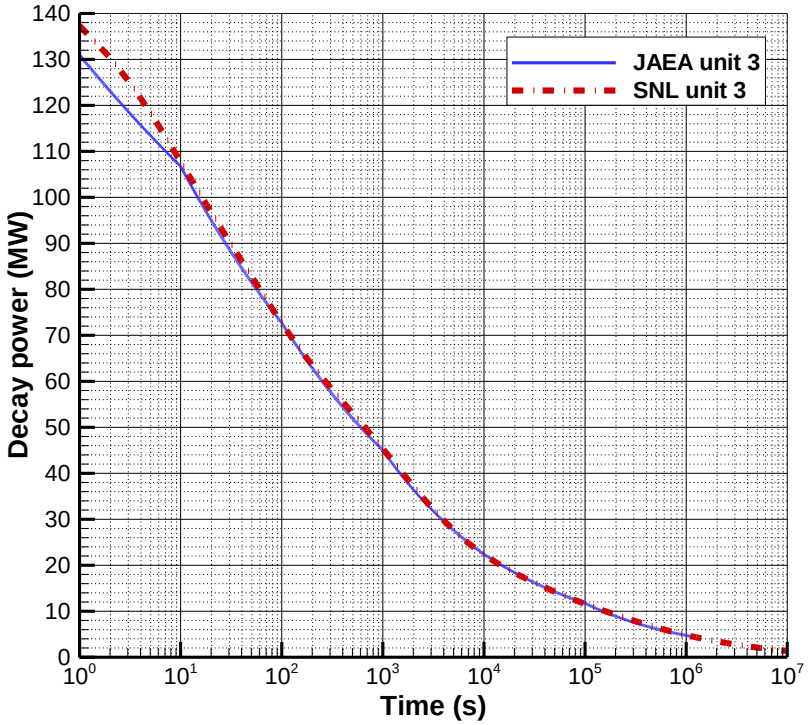

Figure A.5. Unit 3 decay power.

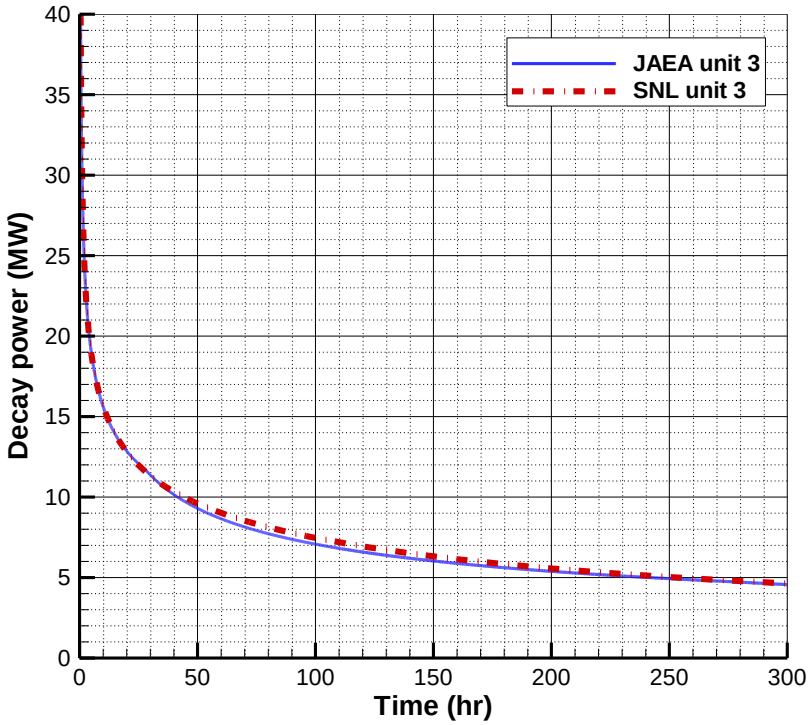

Figure A.6. Unit 3 decay power on severe accident time scale.

A.3 Decay Power Distributions

Radial decay power distributions over the cores of units 1-3 are shown by Figure A.7 and Figure A.8. These figures depict decay power over five rings that radially nodalize the Fukushima cores in the SNL MELCOR models [5]. In Figure A.7, the peaking factors represent the absolute decay power associated with each core ring, which are not of equal size in the SNL MELCOR models. Since ring 3 is the largest in the models, it tends to produce the most decay power. The absolute power factor is the correct figure for spatially allocating lumped RN masses in MELCOR in order to obtain the desired decay power distribution. Because decay power soon after shutdown inherently follows short-lived nuclide concentrations rather than lumped RN mass (comprised largely of stable and long-lived nuclides), this results in a small but acceptable level of modeling error. For instance, the cesium class mass is composed mainly of ^{133}Cs and ^{137}Cs, and hence it would be more correct to concentrate this mass in the outer ring (5) due to its higher average burnup. In Figure A.8, the ring peaking factors are normalized by their respective ring sizes (i.e. the number of fuel assemblies or the gross fuel mass). The radial power distributions are rather similar for the three units when lumped over five coarse rings; still, the unit 3 distribution is a little flatter than the other units. Axial allocation of RN mass is a simpler matter due to the comparability of axial power and burnup distributions. Axial power and burnup distributions were presented in Section 2.2.1 (see Figure 2.5, Figure 2.6, and Figure 2.7).

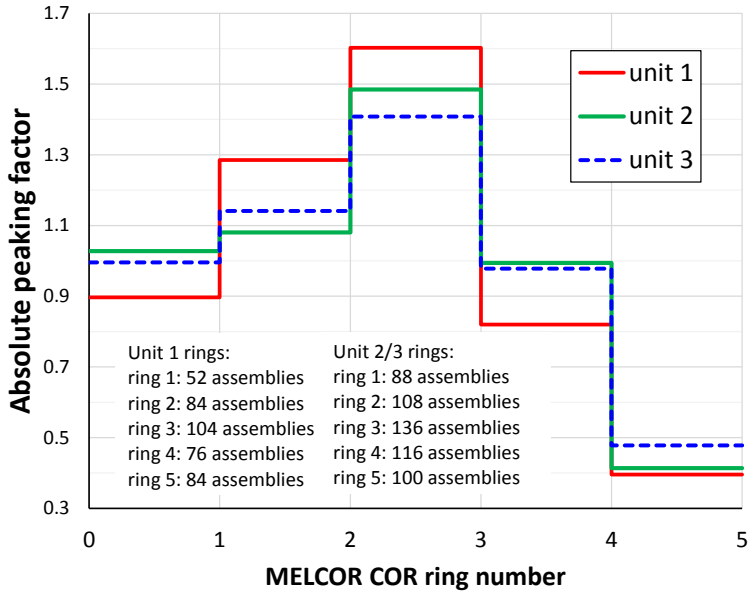

Figure A.7. Decay power distributions for units 1-3.

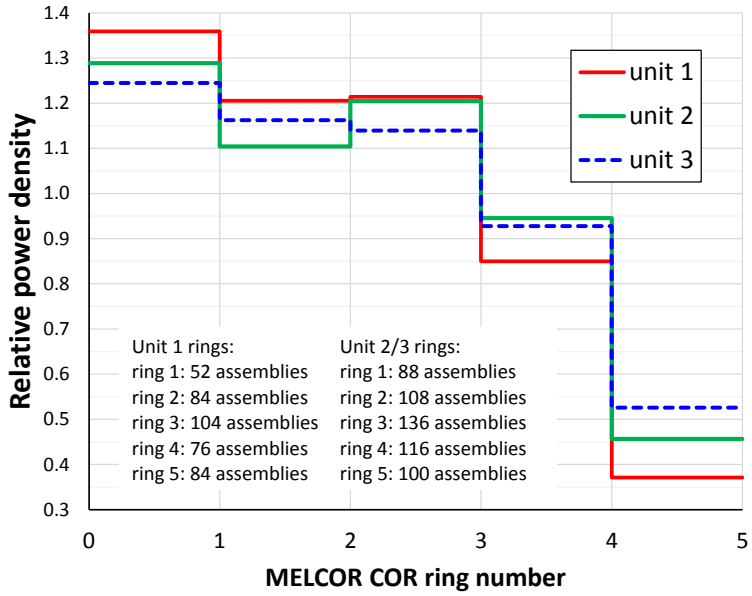

Figure A.8. Decay power density distributions for units 1-3.

A.4 Appendix A References

[1] Sandia National Laboratories, "State-of-the-Art Reactor Consequence Analyses Project Volume 1: Peach Bottom Integrated Analysis," NUREG/CR-7110 Volume 1, USNRC, Washington, DC (2012).

[2] R.O. Gauntt, "Synthesis of VERCORS and Phebus data in Severe Accident Codes and Applications," SAND2010-1633, Sandia National Laboratories (2010).

[3] D.A. Powers, NUREG/CR-4481, "Fission Product Behavior during Severe LWR Accidents: Modeling Recommendations for MELCOR Code System," Volume 1: Fission Product Release from Fuel, SAND85-2743, Sandia National Laboratories, Albuquerque, NM (1988).

[4] R.M. Ostmeyer, NUREG/CR-4169, "An Approach to Treating Radionuclide Decay Heating for Use in the MELCOR Code System," SAND84-1404, Sandia National Laboratories, Albuquerque, NM (1985).

[5] J.N. Cardoni, "Radionuclide Inventory and Decay Heat Quantification Methodology for Severe Accident Simulations," SAND2014-17667, Sandia National Laboratories, Albuquerque, NM (2014).

SAND2016-xxxx

DISTRIBUTION

Internal distribution (electronic copy)

1	MS0748	Nate Andrews	6232
1	MS0748	Jeff Cardoni	6232
1	MS0748	Matt Denman	6231
1	MS0748	Zac Jankovsky	6231
1	MS0899	Technical Library	9536 (electronic copy)

(This page intentionally left blank)


Sandia National Laboratories